Available online at www.sciencedirect.com
SCIENCE DIRECT
ELSEVIER
Coordination Chemistry Reviews 249 (2005) 2854–2879
COORDINATION CHEMISTRY REVIEWS
www.elsevier.com/locate/ccr

Review

Solution structure of chiral lanthanide complexes

Lorenzo Di Bari, Piero Salvadori *

CNR-ICCOM-Sezione di Pisa, Dipartimento di Chimica e Chimica Industriale, Via Risorgimento 35, I-56126 Pisa, Italy

Received 24 September 2004; accepted 4 March 2005
Available online 17 May 2005

Contents

Abstract

The determination of solution structure of small to medium size chiral lanthanide complexes through paramagnetic NMR and circular dichroism is briefly reviewed. The main focus is on ytterbium as the rare earth, because of its negligible contact contribution to the hyperfine shift and of its intense CD spectrum in the near IR. The structures discussed contain various stereogenic elements: classical chiral centres, atropisomeric axes, slowly interconverting conformations, which gives rise to a manifold of situations to be identified, classified, and characterised through spectroscopic tools. The fallout of these structural properties are in enantioselective catalysis, in molecular recognition, or even in biomedicine, on account of the role of Gd^{3+} complexes as MRI contrast agents. Moreover, the information encoded in the NMR and CD spectra of Ln^{3+} complexes may be used to extract original data on the solution stereochemistry of organic molecules used as ligands. The first part summarises some basic theoretical aspects, with special emphasis onto those which have practical consequences in the experimental design. A discussion of selected applications can be found in the second part.

Keywords: Lanthanides; Ytterbium; Chirality; Paramagnetic NMR; Circular dichroism; Near infrared

* Corresponding author. Tel.: +39 050 2219 273; fax: +39 050 2219 409.
E-mail address: psalva@dcci.unipi.it (P. Salvadori).

0010-8545/$ – see front matter © 2005 Elsevier B.V. All rights reserved.
doi:10.1016/j.ccr.2005.03.006

1. Introduction

The use of some spectroscopic properties peculiar to lanthanide (III) ions is an established tool for refined structural investigation in organic as well as in biomolecules. Each element of the series is endowed with different characteristics, but all of them share very similar or nearly identical chemical behaviour: the two properties together offer the investigator the possibility to choose the ion, according to the needs or even to the available equipment; some may take advantage of luminescence, while others may focus on relaxometry. The amplitude of the subject largely justifies the number of review publications which have appeared in the literature. We offer here the contribution of our own experience, primarily centred on ytterbium and based on the combined use of near infrared circular dichroism (CD) and paramagnetic NMR. In both techniques, the presence of the lanthanide opens new spectroscopic windows, where organic molecules, like the free ligand itself, are unlikely to interfere. What follows will necessarily be a very partial account, reflecting our own interests and inclinations, but we aimed at making clear what kind of information one can obtain from the experiments and – possibly – how can one get them work.

The increasing interest towards Ln^{3+} complexes, for example in synthetic organic chemistry, in magnetic resonance tomography, in fluorescence microscopy, in targeted radiotherapy raises a quest for investigation protocols.

The text will be divided in two parts, one dealing with a general description of the methods and of their relevant relations, the other dealing with selected applications.

2. Methods

2.1. NMR: lanthanide induced relaxation and shifts

Lanthanide complexes have been known for a long time as useful auxiliaries in NMR spectroscopy, because they induce significant modifications in solute molecular spectra, with which they interact. The main application is as shift reagents: when the NMR spectrum of a compound is too complicated, for example because of signal overlap, adding a small quantity of a diketonate of e.g. Pr, Eu or Yb, can spread and resolve the signals, by a mechanism defined as a lanthanide-induced shift or LIS. This process is accompanied by a broadening of the analyte resonance lines, referred to as LIR (lanthanide induced relaxation). Interestingly, the enhanced lability of many lanthanide complexes implies that the adduct between the shift reagent and the analyte is in fast exchange with the free species, meaning that upon progressive additions of portions of the paramagnetic complex, one can follow the modification of the analyte spectrum. Modern multidimensional NMR techniques and the diffusion of high-field spectrometers made the use of shift reagents less popular, with the very notable exception of chiral systems. Two enantiomers of a chiral compound have the same chemical potential and consequently have rigorously the same NMR spectrum, unless they interact with a further chiral entity. By establishing labile diastereomeric interactions with the analyte enantiomers, a chiral lanthanide shift reagent (CLSR) may be able to split the resonances of the two forms. This can be exploited to quantitatively assess the enantiomeric composition of a mixture. A few selected lanthanide shift reagents and CLSRs that can be commonly found in the literature are depicted in Fig. 1.

The origin of LIR and LIS resides in the coupling between the nucleus observed through magnetic resonance and the unpaired lanthanide electrons. We shall refer to classical reviews describing the processes underlying these effects and recall here the most relevant results, useful for structural analysis in solution. A much more detailed description can be found by Bertini and Luchinat's book [1], or in other excellent reviews [2].

An aspect seemingly not fully appreciated is that the interactions detailed below occur between a nucleus (e.g. ^{1}H or ^{13}C), which is in a well-determined position in space, and a diffuse electron cloud. One may grossly estimate the extent of such delocalisation for example by means of the 4f orbital radial distribution [3], which indicates an uncertainty of about ± 0.3 Å around the Ln^{3+} nucleus. For small complexes, where some of the relevant nucleus–lanthanide distances are below 4 Å, this means that the dipolar approximation used may be critical and this introduces an error, which may be more serious than neglecting, for example, the contact contribution to the hyperfine shift.

2.1.1. Overview of paramagnetism-enhanced relaxation

Paramagnetism-enhanced relaxation represents the increased rate of nuclear recovery toward equilibrium determined by very efficient fluctuating magnetic fields generated by the unpaired electrons. Since relaxation rates are additive quantities, one can define the lanthanide induced relaxation as the amount exceeding the longitudinal or transverse recovery rate ρ for a given nucleus in an isostructural diamagnetic compound. For a given nucleus

$$\rho^{\text{para}} = \rho^{\text{obs}} - \rho^{\text{dia}} \tag{1}$$

where ρ^{obs} is the observed relaxation rate, ρ^{dia} is the analogous quantity for a reference diamagnetic complex. Eq. (1) holds for longitudinal as well as for transverse relaxation; thus, properly speaking one would be able to introduce two distinct effects for the same nucleus. The reference compound can be taken most correctly as the lanthanum or lutetium complex. Very often, one makes use of the term lanthanide induced relaxation, LIR, which may be unsatisfactory in some cases: LIR is defined as the difference

$$\text{LIR} = \rho^{\text{obs}} - \rho^{\text{free}}$$

and equating ρ^{para} to LIS implies that $\rho^{\text{dia}} = \rho^{\text{free}}$, which may be incorrect for nuclei very close to donor atoms or when coordination implies a structural readjustment. In the

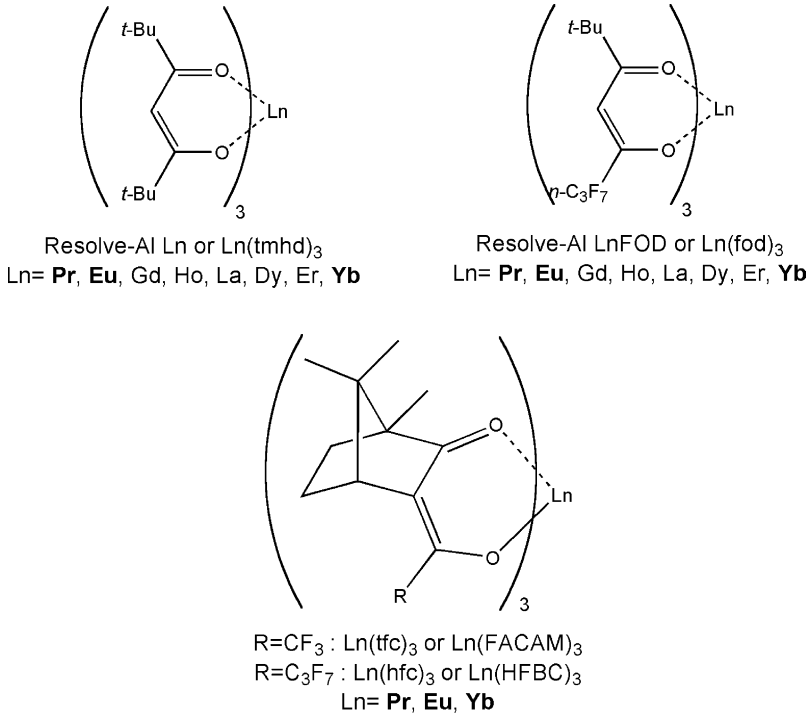

Fig. 1. Common achiral (top) and chiral (bottom) lanthanide shift reagents. In bold are indicated the most commonly occurring lanthanides.

context of shift reagents, instead, the term LIR is completely adequate.

Electron and nucleus are coupled by dipolar interaction, through two different mechanisms; in the first place electron and nucleus are two particles with non-vanishing spin magnetic moments (this will be referred to as dipolar relaxation); secondly, given its long lifetime, the nucleus senses the average magnetic moment of the molecule, which in turn is responsible for its macroscopic magnetic susceptibility (Curie relaxation).

Magnetic relaxation is described through spectral density functions, which in turn contain a correlation time. In the following we shall review the relevant correlation times and what reasonable values should be expected.

In small to medium-size molecules, the diamagnetic contribution ρ^{dia} can roughly be estimated to 0.5–2 s^{-1}: given the large values usually found for ρ^{obs}, any deviation from this guess introduces only a minor error in ρ^{para}. The two main interactions leading to enhanced relaxation discussed below lead to the same expression

$$\rho_{1,2} = \frac{A_{1,2}(\tau_{\mathrm{c}})}{r^6} \tag{2}$$

that is, both longitudinal and transverse rates are phenomenologically proportional to r^{-6}. The values of the constants $A_{1,2}$ and the relevant correlation time τ_{c} depend on the specific mechanism, as discussed below.

2.1.1.1. Dipolar interaction. A given nucleus is under the effect of the magnetic field generated by the unpaired electron(s); this interaction is described through the equation of a dipolar coupling. In the case of paramagnetic lanthanides (Ce^{3+}–Yb^{3+}) and with the exception of Gd^{3+}, the most relevant correlation time τ_{c} describing the random fluctuations of the electron–nuclear dipolar interactions is the very short electronic relaxation time $\tau_{\mathrm{c}} = \tau_{\mathrm{s}} \approx 10^{-13}$ s. This value implies that $(\omega\tau_{\mathrm{c}})^2 \ll 1$ (low field limit) practically at most fields currently used for NMR. This simplifies the equations for nuclear relaxation: the longitudinal and transverse rates for the nucleus I become equal and can be written as

$$\rho_1^{\mathrm{dip}} = \rho_2^{\mathrm{dip}} = \frac{4}{3}\left(\frac{\mu_0}{4\pi}\right)^2 \frac{\gamma_I^2 g_J^2 \mu_{\mathrm{B}}^2 J(J+1)\tau_{\mathrm{s}}}{r^6} = \frac{A^{\mathrm{dip}}(\tau_{\mathrm{s}})}{r^6} \tag{3}$$

where γ_I is the nuclear magnetogyric ratio for I, μ_{B} is the electron Bohr magneton J is the appropriate quantum number for the lanthanide ion, g_J the associated g-factor. Properly, r is the electron–nucleus distance and assumes that a point-dipole approximation is valid, i.e. that the unpaired electron(s) cloud can be effectively described as a point, fixed in space. This is usually valid for nuclei 4 Å away and excluding extensive electron delocalisation onto the ligands. In such a hypothesis, r can be substituted by the nucleus–Ln^{3+} distance.

Owing to the high symmetry of the $4f^7$ configuration, the electronic relaxation time of Gd^{3+} is several orders of magnitude longer.

2.1.1.2. Curie mechanism. The second relevant mechanism of nuclear relaxation in paramagnetic systems proceeds through the coupling of the nuclear spin with the average magnetic moment of the whole molecule. This derives from the (small) electron polarisation in the external field B_0,

which is responsible for the magnetic susceptibility (hence the name "Curie relaxation"). It is immediately clear that this mechanism is magnetic field and temperature dependent. The stochastic process modulating the magnitude of the random field ensuring nuclear relaxation, is molecular tumbling. The relevant correlation time is thus the reorientation time $\tau_c = \tau_R$. This can be approximately predicted through the Stokes equation

$$\tau_R = \frac{4\pi\eta a^3}{3kT}\frac{\eta M_R}{dN_A kT} \quad (4)$$

with η the viscosity of the solution, a the radius of the molecule (supposed spherical), M_R the molecular weight and d the density of the solute, N_A the Avogadro's constant. In water, at 25 °C, $\tau_R \approx 30 \times 10^{-12}$ s for aquo ions and $\tau_R \approx 80 \times 10^{-9}$ s for a small protein (10 kDa). Thus, depending on the molecular size and on the solution properties, the rotational correlation time may or may not be compatible with a fast motion-low field approximation.

The full equations for longitudinal and transverse rates are

$$\rho_1^{Curie} = \frac{2}{5}\left(\frac{\mu_0}{4\pi}\right)^2 \frac{\omega_I^2 g_J^4 \mu_B^4 J^2(J+1)^2}{(3kT)^2 r^6}\left(\frac{3\tau_R}{1+\omega_I^2\tau_R^2}\right) \quad (5)$$

$$\rho_2^{Curie} = \frac{1}{5}\left(\frac{\mu_0}{4\pi}\right)^2 \frac{\omega_I^2 g_J^4 \mu_B^4 J^2(J+1)^2}{(3kT)^2 r^6}\left(4\tau_R + \frac{3\tau_R}{1+\omega_I^2\tau_R^2}\right) \quad (6)$$

where ω_I is the Larmor frequency of the nucleus I. It is equal to

$$\omega_I = \gamma_I B_0 \quad (7)$$

which makes explicit the external magnetic field dependence of Curie relaxation rates.

Whenever $(\omega_I\tau_R)^2 \ll 1$ the above equations simplify to

$$\rho_1^{Curie} = \frac{6}{5}\left(\frac{\mu_0}{4\pi}\right)^2 \frac{\omega_I^2 g_J^4 \mu_B^4 J^2(J+1)^2\tau_R}{(3kT)^2 r^6} = \frac{A_1^{Curie}\tau_R}{r^6} \quad (8)$$

$$\rho_2^{Curie} = \frac{7}{5}\left(\frac{\mu_0}{4\pi}\right)^2 \frac{\omega_I^2 g_J^4 \mu_B^4 J^2(J+1)^2\tau_R}{(3kT)^2 r^6} = \frac{A_2^{Curie}\tau_R}{r^6} \quad (9)$$

The two rates are therefore different even within the low field regime. This is in contrast with that which was reported above for dipolar relaxation and has been used to determine a quantity depending only on τ_R and on r^{-6}

$$\rho_2^{obs} - \rho_1^{obs} = \rho_2^{Curie} - \rho_1^{Curie} = \frac{1}{5}\left(\frac{\mu_0}{4\pi}\right)^2 \frac{\omega_I^2 g_J^4 \mu_B^4 J^2(J+1)^2\tau_R}{(3kT)^2 r^6} \quad (10)$$

In fact, for diamagnetic and dipolar relaxation, in the low field regime, the longitudinal and transverse rates are equal and cancel out. The advantage of this procedure is that one can consider τ_R as known, either through the gross assessment provided by Stokes equation (4), or through its experimental determination in diamagnetic systems (e.g. with the La or Lu complexes). The easiest way is through a ^{13}C-T_1 measurement of a C–H system, recorded while saturating ^{1}H. Provided nuclear dipolar relaxation is the main process,[1]

$$\tau_R(ps) = 49.4T_1^{-1}(s^{-1}) \quad (11)$$

where T_1 is the ^{13}C longitudinal relaxation time. The quantity τ_R contains an implicit dependence on T, which has two different and important sources: the rotational dynamics of solute molecular tumbling (appearing in the Stokes equation (4)), and the viscosity η of the solution. Curie relaxation is more strongly influenced by temperature than the inverse square proportionality made explicit in Eqs. (8) and (9), and arising from Curie law of magnetic susceptibility.

Unfortunately, obtaining the transverse rate required in Eq. (10) may be far from trivial for lanthanide complexes. In fact, the linewidth is often not much larger than in diamagnetic system, provided chemical exchange can be ruled out, as discussed below. Thus, broadening due to B_0 inhomogeneity and to partially unresolved scalar couplings may prevent estimation of ρ_2 from the linewidth and one should resort to specific sequences.[2]

Typical expected paramagnetic linewidths for a small complex, of the size of a tris diketonate or of LnDOTA$^-$ throughout the lanthanide series can be determined through Eqs. (9) and (3), and are reported in Table 1.

2.1.1.3. Chemical exchange and EXSY spectra. The NMR spectrum can be very sensitive to the dynamic processes the molecules undergo. Fast and slow exchange regimes take up a particular meaning, when dealing with paramagnetic systems: as we shall see below, a structural rearrangement may be accompanied by very large pseudocontact (and possibly also contact) shifts. Moreover, any free/bound equilibrium implies that a given nucleus is under the influence of chemical shift in the free form, while it experiences a very large hyperfine shift once bound. Thus, it is rather common that even at room temperature the dynamic processes fall in the slow exchange limit ($k < 2\pi\omega_0\Delta\delta$, with ω_0 the Larmor frequency) and separate NMR spectra are detected for the two forms. This is notably the case of ring inversion and side arm rotation in DOTA derivatives [4], discussed in Section 3.3, as well as of the metal binding equilibria in anthracyclins [5,6]. Slow exchange (in the NMR context) means that one may be

[1] This can be easily verified by comparing the entity of Overhauser enhancement. To this end, one must record two ^{13}C spectra one with and one without proton irradiation prior to acquisition. The relaxation delay must be longer than $5T_1$ in both cases. The Overhauser enhancement η is the intensity ration for the same peak in the two spectra. If $\eta = \gamma_H/\gamma_C - 1 = 2.99$, ^{13}C relaxation is purely dipolar.

[2] While writing this contribution, Dr. Guido Pintacuda drew our attention to the fact that transverse relaxation might be seriously affected by chemical shift anisotropy/Curie cross correlation. If this mechanism provides a significant further line broadening, Eq. (10) might be incorrect. Further investigation on this issue will be required.

Table 1
Expected contributions to the ^{1}H NMR linewidths (Hz) of a kinetically inert lanthanide complex calculated through Eqs. (3) and (9)

Nucleus	J	g_J	τ_s (ps)	Dipolar	Curie (7 T)	Curie (14.1 T)
Ce	5/2	6/7	0.5	5.4	0.20	0.81
Pr	4	4/5	0.5	10.7	0.80	3.2
Nd	9/2	8/11	0.5	10.9	0.83	3.4
Sm	5/2	2/7	0.5	0.6	0.0025	0.0099
Tb	6	3/2	0.69	109	43	176
Dy	15/2	4/3	0.82	155	62	249
Ho	8	5/4	0.54	102	61	250
Er	15/2	6/5	0.85	130	41	166
Tm	6	7/6	1.54	147	16	64
Yb	7/2	8/7	0.28	9.6	2.0	8.3

The Curie term is evaluated at two different B_0 fields. The Ln–H distance r is assumed 5 Å, and $\tau_R = 100$ ps; the electronic correlation time τ_s for the late lanthanides has been taken from Ref. [13] and arbitrarily set to 0.5 ps for the others. Pm, Eu, Gd are not reported: the first is a synthetic element and strongly radioactive, Eu^{3+} has $J = 0$ in its ground state and Gd^{3+} has a $\tau_s \approx 10^{-8}$ to 10^{-9} s, leading to an exceedingly large dipolar term (the linewidth $\Delta\nu$ (Hz) is related to the transverse relaxation rate ρ_2 through $\Delta\nu = \rho_2/\pi$).

able to record EXSY spectra, under the condition that appreciable exchange take place within the longitudinal magnetisation lifetime; this puts a further restriction: $k > 5\rho_1$. EXSY spectra can be recorded with the conventional NOESY sequence, with the only precaution of adjusting the mixing time. Often, for Yb complexes 10–100 ms are reasonable values. ROESY sequence can in principle be used, as well. Especially in macromolecular diamagnetic systems, with long tumbling time, this has the advantage that exchange and Overhauser cross-peaks are oppositely signed and can thus be easily distinguished. Unfortunately, with proton spectra spanning several tens of ppm's, strong spin-lock fields need to be applied in order to effectively cover the whole spectral width. This may induce sample heating and TOCSY-artefacts. Quantitative analysis of EXSY spectra at variable mixing time t_{mix} can provide exchange rates. In fact, given a pair of exchanging proton signals, at υ_1 and υ_2, in the 2D spectrum one observes four peaks at the frequency pairs (υ_1, υ_1), (υ_1, υ_2), (υ_2, υ_1), (υ_2, υ_2), whose volume integrals can be arranged in a matrix **A**. Perrin and Gipe [7] demonstrated that **A** is related to the exchange matrix **L** through the equation

$$\mathbf{L} = \frac{1}{t_{mix}} \ln(\mathbf{P}^{-1}\mathbf{A}) = \frac{1}{t_{mix}} \mathbf{U}^{-1} \ln(\mathbf{\Lambda})\mathbf{U} \quad (12)$$

where **U** is the matrix of eigenvectors and the diagonal matrix **Λ** contains the eigenvalues Λ_{ii}, of ($\mathbf{P}^{-1}\mathbf{A}$). The diagonal matrix $\mathbf{P}^{-1}$ contains the population of the exchanging species, so that the elements of ($\mathbf{P}^{-1}\mathbf{A}$) are the normalised amplitudes of the peaks.

For obtaining exchange rates, one can also follow steady state nOe build up, through saturation transfer experiments. In both cases, one takes advantage of the dispersion of signals brought about by hyperfine shifts.

EXSY spectra can be particularly valuable in the case of free/bound exchange, because they allow a fast and straightforward way of assigning the paramagnetic NMR spectrum from knowledge of the shifts for the molecule in the free state. In this case, cross-peaks are confined in a cross, spanning 0–12 ppm in one dimension (the normal diamagnetic spectrum) and a much wider area in the other. By a careful choice of transmitter offset and of spectral width in f_1, one may acquire a rectangular EXSY spectrum with improved digital resolution in the first dimension. Obviously, care must be taken with folded signals.

Fast or intermediate exchanges are typical of situations where no conformational rearrangement of ligand or of the paramagnetic complex occurs and it is particularly significant when the lanthanide chelate has a labile axial site. This is indeed the case for shift reagents, for catalysts and notably for analogues of MRI contrast agents. All these can be regarded as functional molecules, specifically designed to ensure weak reversible binding, usually to oxygen-containing functional groups, like hydroxyls, carbonyls, carboxylates. The NMR spectrum contains one set of lines falling at a shift, which is the average of the two exchanging forms, weighted for the relative populations. This means that the observed shifts depend on the solution composition and can be brought from one form to the other by displacing the position of the equilibrium. Typically, with shift reagents, one starts with the free analyte, then adds small portions of the lanthanide chelate, following the stepwise displacement of each signal.

Intermediate exchange, occurring when $k \approx 2\pi\omega_0\Delta\delta$ manifests itself through extensive line broadening. A glance at the values of expected ^{1}H linewidths for inert lanthanide complexes reveals that at least at intermediate fields and for molecules of smaller size, the largest values are of the order of 60 Hz, only for Dy and Ho, provided one focuses on protons distant 5 Å. Any major increase (and most notably for nuclei like Yb or Eu) must be attributed to dynamic processes of some sort. This is indeed the case of labile axial coordination, which will be treated in some detail in Section 2.3.1.

2.1.2. Contact and pseudocontact shifts

Hyperfine or paramagnetic shift is defined through the equation

$$\delta^{para} = \delta^{obs} - \delta^{dia} \quad (13)$$

By analogy to LIR, discussed in Section 2.1.1, and with the same precautions in its use, one can define a lanthanide induced shift, LIS, as

$$LIS = \delta^{obs} - \delta^{free}$$

The paramagnetic shift is the sum of two contributions called contact and pseudocontact shifts

$$\delta^{para} = \delta^{c} + \delta^{pc} \quad (14)$$

The former arises from the probability of finding the electron localised onto the observed nucleus, and this is the reason why it is also called Fermi contact shift. This property is transmitted through covalent bonds and, because lanthanides

give usually rise to a mostly electrostatic bonds, δ^c can be neglected for nuclei distant more than 4–5 bonds from the paramagnetic centre (unless involved in extensive conjugation). δ^c is strongly reminiscent of a scalar J coupling in diamagnetic NMR and, likewise, it is a function of the geometry. For three-bond systems, it follows a Karplus-like trend, with a maximum for antiperiplanar arrangements. Indeed this is what Forsberg et al. reported in the most thorough analysis of LnDOTAM hyperfine shifts [10]. However, systematic investigations of Ln–^{1}H contact shifts are still scarce and there is no quantitative relationship to the geometry. On the contrary, the pseudocontact term is directly dependent on the structure and on the magnetic anisotropy of the ion.

The anisotropic electronic distribution of a paramagnetic lanthanide differing from Gd^{3+} in an external field $\mathbf{B_0}$ gives rise to a magnetic dipole moment $\boldsymbol{\mu}$, which is proportional to the field through a magnetic susceptibility tensor $\tilde{\boldsymbol{\chi}}$:

$$\boldsymbol{\mu} = \tilde{\boldsymbol{\chi}}'\mathbf{B_0} \tag{15}$$

Therefore, in a generic point (x, y, z) at a distance r from the centroid of the electronic distribution, there will be an additional magnetic field expressed by

$$\mathbf{B}' = \frac{\boldsymbol{\mu}}{r^3} - \frac{3(\boldsymbol{\mu}\cdot\mathbf{r})\mathbf{r}}{r^5} = \tilde{\mathbf{T}}\boldsymbol{\mu} \tag{16}$$

where we introduced the dipolar tensor

$$\tilde{\mathbf{T}} = \frac{1}{r^5}\begin{pmatrix} 3x^2 - r^2 & 3xy & 3xz \\ 3xy & 3x^2 - r^2 & 3yz \\ 3xz & 3yz & 3x^2 - r^2 \end{pmatrix} \tag{17}$$

$\mathbf{B}' = \tilde{\mathbf{T}}\tilde{\boldsymbol{\chi}}'\mathbf{B_0}$ adds to $\mathbf{B_0}$ in the Zeeman Hamiltonian. The observed contribution to the shift induced by this term is the motional average of $\mathbf{B}'$, thus for isotropic reorientation, one has to take the trace of $\tilde{\mathbf{T}}\tilde{\boldsymbol{\chi}}'$. Observing that $\tilde{\mathbf{T}}$ is a traceless tensor one must introduce

$$\tilde{\boldsymbol{\chi}} = \tilde{\boldsymbol{\chi}}' - \mathrm{tr}(\tilde{\boldsymbol{\chi}}')\mathbf{1}$$

Using the Cartesian components (in a molecule-fixed coordinate system) of the susceptibility tensor, the pseudocontact contribution to the shift is written

$$\delta^{pc} = -\mathrm{tr}(\tilde{\mathbf{T}}\tilde{\boldsymbol{\chi}}) = -\frac{1}{r^5}\left[\left(\chi_{zz} - \frac{\chi_{xx}+\chi_{yy}}{2}\right)(3z^2 - r^2) + \frac{\chi_{xx}-\chi_{yy}}{2}(3x^2 - 3y^2) + 6\chi_{xy}xy + 6\chi_{xz}xz + 6\chi_{yz}yz\right] \tag{18}$$

and shows a dependence on 5χ parameters. If the Cartesian axes are chosen along the principal directions of $\tilde{\boldsymbol{\chi}}$, the cross terms, like χ_{xy}, vanish, and one can obtain the simplified expression

$$\delta^{pc} = D_1\frac{1 - 3\cos^2\theta}{r^3} + D_2\frac{\sin^2\theta\cos 2\varphi}{r^3} \tag{19}$$

with the parameters $D_1 = \chi_{zz} - 1/2(\chi_{xx} + \chi_{yy})$; $D_2 = 3/2(\chi_{xx} - \chi_{yy})$ and (r, θ, φ) the polar coordinates of the nucleus under examination with respect to the electronic spin in the principal axes system of $\tilde{\boldsymbol{\chi}}$.

Molecular symmetry can simplify the task of finding the principal axes of $\tilde{\boldsymbol{\chi}}$. Thus, in C_2 symmetric molecules, one principal axis must lie along the C_2, and for D_2 the three directions are completely defined. With a C_3 symmetry (or higher), the molecule appears totally axially symmetric, i.e. $\chi_{xx} = \chi_{yy}$. This further reduces Eq. (19) to

$$\delta^{pc} = D\frac{3\cos^2\theta - 1}{r^3} \tag{20}$$

This relation is sometimes referred to as the McConnel–Robertson equation and, in the context of shift reagents, Eq. (20) has been used often, irrespective of the real symmetry of the intermolecular adduct between the analyte and the lanthanide system [2a] This can be justified for molecules containing one monodentate binding site, because of a dynamic rotational process, which provides an *effective* axial symmetry.

The relationship between the magnetic susceptibility anisotropy and crystal field parameters has been investigated by Bleaney [8] and more recently by Mironov et al. [9].

2.1.2.1. Separation of the contributions. As expressed in Eq. (14), the total paramagnetic shift is the sum of the two contributions δ^{pc} and δ^c, neither of which is known or easily predictable. Since only the former contains relevant geometric information, quantitative structural analysis requires a reliable separation of the observed shift into contact and pseudocontact terms. The problem has been faced by many authors and we shall describe here only some of the methods proposed to this end. We have already demonstrated that δ^{pc} is a linear combination of products of geometric terms and of magnetic susceptibility constants. Its most compact – although general – form is expressed in Eq. (19), which is valid only if we know the directions of the principal axes of $\tilde{\boldsymbol{\chi}}$.

It has been demonstrated that in a series of isostructural complexes, scanning the lanthanide ion j, the contact contribution δ^c_{ij} for each nucleus i follows a regular trend:

$$\delta^c_{ij} = F_i \cdot \langle S_z\rangle_j \tag{21}$$

The terms $\langle S_z\rangle_j$ are rather insensitive to the specific complex and have been calculated throughout the series [1]. Thus one can write:

$$\delta^{para}_{ij} = F_i \cdot \langle S_z\rangle_j + (D_{1j}G_{1i} + D_{2j}G_{2i}) \tag{22}$$

where G_{1i} and G_{2i} are the two geometric factors appearing in Eq. (19). The problem is thus partitioned in factors, depending only on the nucleus i (F_i, G_{1i}, G_{2i}) and only on the lanthanide ion j ($\langle S_z\rangle_j$, D_{1j}, D_{2j}). A whole set of δ^{para}_{ij} can be collected for a whole set of nuclei.

Table 2
Values of $\langle S_z \rangle$ throughout the Ln^{3+} series [1]

Ce	Pr	Nd	Sm	Eu	Tb	Dy	Ho	Er	Tm	Yb
0.98	2.97	4.49	−0.06	−10.68	−31.82	−28.54	−22.36	−15.37	−8.21	−2.59

Elegantly, Forsberg et al. [10] observed that the above equation is the scalar product

$$\delta_{ij}^{\text{para}} = \mathbf{Q_i} \cdot \mathbf{P_j^T} \tag{23}$$

where $\mathbf{Q_i} = (F_i, G_{1i}, G_{2i})$ and $\mathbf{P_j} = (\langle S_z \rangle_j, D_{1j}, D_{2j})$.

Eq. (23) is invariant for all i and j values under the introduction of the non-singular 3×3 transformation matrix $\mathbf{D}$

$$\delta_{ij}^{\text{para}} = \mathbf{Q_i} \cdot \mathbf{D} \cdot \mathbf{D}^{-1} \mathbf{P_j^T} \tag{24}$$

which means for any choice $\mathbf{Q_i}' = \mathbf{Q_i} \cdot \mathbf{D}$ and $\mathbf{P_j}' = (\mathbf{D}^{-1})^{\text{T}} \cdot \mathbf{P_j}$. This demonstrates that the problem as such has infinite equivalent solutions and that further elements have to be sought in order to make a choice among them (this is in fact a gauge choice).

The simplest approach is to assume a structure, which means to fix G_{1i} and G_{2i},[3] a strategy followed for example by Kemple et al. [11].

Forsberg et al. investigated a C_4-symmetric complex, analogue to DOTA [10]. In this case, the McConnel–Robertson equation holds and only one D_j parameter needs to be determined for each lanthanide. In a first approximation, they determined the various F_i, thus obtaining the δ^{c} contributions, by fixing the geometrical factor for one proton (i.e. assuming the geometry for that fragment) and varying all the D_j's, through a multiparameter (10 D_j's and 10 F_i's) fitting of 10×10 $\delta_{ij}^{\text{para}}$ values. The ^{1}H-δ^{c}'s reported by Forsberg et al. confirm that:

- in the Yb^{3+} complex, they are a small fraction of the total shifts, for almost all protons;
- the most affected nuclei are vicinal and antiperiplanar to Yb.

Lisowski et al. [12] took a heuristic approach for analysing the spectra of Ln^{3+} texaphyrins, by excluding from a structural fit those nuclei which were likely to be affected from non-negligible contact interaction. By so doing, they determined a magnetic susceptibility tensor, which was in turn used for calculating the δ^{pc}'s for all the nuclei and finally to retrieve the δ^{c}'s for all the nuclei.

In complete alternative to these approaches, one may assume that the D_{nj} ($n = 1, 2$) parameters follow Bleaney's theory (see Section 2.3) and can be predicted accordingly. We shall not discuss this point any further, because such assumptions have recently met some criticism, based (1) on the validity of the theory [9]; (2) on the invariance of crystal field parameters throughout the series [2b,13,14].

For axial complexes, one can eliminate the parameter D by means of two equations (22) for nuclei i and k, obtaining [15]

$$\frac{\delta_{ij}^{\text{para}}}{\langle S_z \rangle_j} = \left(F_i - F_k \frac{G_i}{G_k} \right) + \frac{G_i}{G_k} \cdot \frac{\delta_{kj}^{\text{para}}}{\langle S_z \rangle_j} \tag{25}$$

This means that plotting $\delta_{ij}^{\text{para}}/\langle S_z \rangle_j$ against $\delta_{kj}^{\text{para}}/\langle S_z \rangle_j$ along the series of lanthanide ions j, one should obtain a straight line with slope G_i/G_k and intercept $F_i - F_k(G_i/G_k)$, provided the complexes are isostructural. Assuming that at least one geometric parameter G_k or one contact shift F_k is known, one can solve the whole problem graphically. This latter requirement is exactly equivalent to Forsberg's gauge mentioned above. Indeed this latter method has the merit of providing a simple expression amenable to linear plots, although it is mathematically equivalent to Forsberg's: its advantage lies in the immediate evidence of deviations from the expected trend, which can be related to structural variations along the series.

Once we accept that the contact shifts are proportional to $\langle S_z \rangle$, we can evaluate the contribution for the various Ln^{3+} according to the values of Table 2. As a reminder, for a vicinal proton three bonds apart from Yb, in an *anti*-conformation a value $\delta^{\text{c}} \approx 4$–5 ppm is expected.

2.1.2.2. Structural inference through pseudocontact shifts and relaxation rates. The complete problem of solving a geometry for a set of N atoms consists in determining $(3N–6)$ coordinates. It can be reduced by imposing constraints, like internuclear distances and angles. By doing so, the number of variables is greatly reduced and it may be sufficient to consider only dihedral angles as real fitting parameters. Paramagnetic NMR provide a wealth of experimental data rich in structural information: Eqs. (18) and (3)–(10) provide experimental constraints that can be used in a global optimisation of:

- The five components of the magnetic susceptibility tensor $\tilde{\boldsymbol{\chi}}$.
- The correlation time (rotational, electronic or both), τ_{c}.
- The location of the lanthanide ion.
- A set of dihedrals on the organic ligand.

This approach avoids any assumption on molecular geometry or, equivalently, any bias arising from symmetry. Interestingly protons and carbon pseudocontact shifts and

[3] To be precise, in the absence of symmetry elements defining the principal axes of the magnetic susceptibility tensor, one should go through more complicated equations, which are anyway formally equivalent to what is presented here, and can be derived in the same way as we did for Eqs. (22)–(24), but starting from the full equation (18).

relaxation rates provide a very large number of experimental constraints. Recently we developed a Fortran routine, called PERSEUS, which performs such a non-linear fitting, by minimising the functional

$$F = \frac{\sum_{i=1}^{s} A_i(\delta_i^{\mathrm{pc(calc)}} - \delta_i^{\mathrm{pc(exper)}})^2}{\sum_{i=1}^{s}(\delta_i^{\mathrm{pc(exper)}})^2} + \frac{\sum_{j=1}^{r} B_j(\rho_j^{\mathrm{par(calc)}} - \rho_j^{\mathrm{par(exper)}})^2}{\sum_{j=1}^{r}(\rho_j^{\mathrm{par(exper)}})^2} + \frac{\sum_{k=1}^{t} C_k(r_{k(\mathrm{Ln-D})} - \langle r_{k(\mathrm{Ln-D})}\rangle)^2}{\sum_{k=1}^{t}\langle r_{k(\mathrm{Ln-D})}\rangle^2} \quad (26)$$

In this equation the three sums go over the s pseudocontact shifts, the r relaxation rates, and the t donor atoms D, respectively. Each piece of information can be independently weighted through the factors A_i, B_j, C_k. The Ln–D distance has been added as a further possibility, because, especially when relaxation rates are not available the shift information alone does not determine accurately the position: one can thus impose optimal values for such parameters by inserting $\langle r_{k(\mathrm{Ln-D})}\rangle$. The program uses the steepest descent to minimise F by varying the five independent components of $\tilde{\boldsymbol{\chi}}$ appearing in Eq. (18), a phenomenological constant A as indicated in Eq. (2), which contains a linear combination of τ_s and τ_R, the location of the Ln^{3+} ion, a set of dihedral angles along single bonds. Once the five the tensor $\tilde{\boldsymbol{\chi}}$ is known, one can retrieve its principal axis system by a simple diagonalisation. The direction of these axes can provide further structural parameters, as we shall see in Section 3.2.

Eq. (26) is nothing else than a generalisation of the so-called agreement facto, sometimes indicated as AF or R and usually expressed as a %. In fact, for pseudocontact shifts alone, this factor is

$$R = \sqrt{\frac{\sum_{i=1}^{s}(\delta_i^{\mathrm{pc(calc)}} - \delta_i^{\mathrm{pc(exper)}})^2}{\sum_{i=1}^{s}(\delta_i^{\mathrm{pc(exper)}})^2}} \quad (27)$$

that is, with all the weights $A_i = 1$ and B_j, $C_k = 0$.

One of the most thorough and critical reports is due to Kemple et al. [11] who analysed field and temperature-dependent shift and relaxation data for a set of EDTA and benzyl-EDTA complexes along the Ln^{3+} series. These authors used MM2-optimised molecular structures, kept fixed during the non-linear fitting process, which thus optimised only the χ tensor.

Forsberg et al. [10] faced the problem of optimising the structure of an amide derivative of $LnDOTA^-$, after isolating the pseudocontact contribution to δ^{para}, as outlined above. To this end, they treated the z-coordinate of the lanthanide ion as an adjustable parameter, thus obtaining a set of Ln–O and Ln–N distances, which are in good agreement with the expectations of the lanthanide contractions. The SHIFT ANALYSIS program set up by Forsberg contributes to solving the problem of spectra interpretation, by performing a permutation of assignment over all the nuclei.

A simpler treatment was used by Meskers and Dekkers for analysing the intermolecular adduct between $Ln(DPA)_3^{3-}$ (DPA = 2,6-pyridine dicarboxylate, Ln = Tb, Gd) and three vitamin B_{12} derivatives [16]. They assumed the conformation of the corrinoids under investigation from X-ray data and that the magnetic susceptibility tensor in the adduct is the same as in the unbound $Ln(DPA)_3^{3-}$. All that needs to be determined is the location and the orientation of the lanthanide complex and the mole fraction x of the adduct. Indeed, in a free-bound equilibrium, and within the approximation of effective axial symmetry, x acts as a scale factor of the D parameter of McConnel–Robertson equation (20)

$$\delta^{\mathrm{obs}} = (1-x)\cdot\delta^{\mathrm{free}} + x\cdot(\delta^{\mathrm{dia}} + \delta^{\mathrm{para}}) \cong \delta^{\mathrm{free}} + x\cdot\delta^{\mathrm{para}} = \delta^{\mathrm{free}} + x\cdot D\frac{3\cos^2\theta - 1}{r^3} \quad (28)$$

where the second equality holds only with the approximation $\delta^{\mathrm{dia}} = \delta^{\mathrm{free}}$.

The results of this investigation will be discussed in Section 3.4.

This approach is reminiscent of earlier reports, which aimed at analysing the stereochemistry of organic molecules through the exploitation of paramagnetic shifts [17].

Finally, a complex routine, called PSEUDYANA, was developed by Bertini's group [18] as an attachment to a software for protein structure elucidation through (diamagnetic) NMR data. In this case the functional space of torsion angles is explored through a simulated annealing procedure. In other words, PSEUDYANA adds a pseudopotential U_{pc} to the functional describing the conformational energy to be minimised. This is done by introducing a weight w_i for each experimental pseudocontact shift $\delta_i^{\mathrm{pc,exp}}$ and a global scaling factor, which determines the overall weight of the piece of information provided by pseudocontact shifts with respect to the target functional:

$$U_{\mathrm{pc}} = W_{\mathrm{pc}}\sum_i w_{\mathrm{pc}}(\delta_i^{\mathrm{pc(calc)}} - \delta_i^{\mathrm{pc(exper)}})^2 \quad (29)$$

The position of the metal ion and the magnetic anisotropy tensor are then allowed to vary during the calculation in order to minimise the global target functional, which includes conformational energy, as well as experimental constraints.

Interestingly, in spite of the wealth of information one can obtain from pseudocontact shifts and relaxation rates, the solution structure may not be completely defined. This is indeed the case for some DOTA derivatives, as discussed below, in Section 3.3: two different structures have the same set of geometrical factors and Ln^{3+}–nuclei distances (within the experimental error) and cannot be distinguished. The problem can be resolved only with the aid of a proton Overhauser effect and demonstrates that all the manifold of NMR experiments

ought to be used and that in spite of the very efficient relaxation brought about by paramagnetism, small but significant NOEs can be measured also in small complexes.

As a general rule, it is widely accepted that the smaller the agreement factor, the better. This is trivially true, but only to a certain extent: for example, all the uncertainties on the diamagnetic or contact contributions to the shift, or the error introduced by using a point dipole approximation to describe what is in fact a diffused electron spin distribution, justify a certain discrepancy between calculated and experimental shifts: pushing the fitting procedure beyond that limit is meaningless. Unfortunately, it is very difficult, and we are sure not able to, to define in general where and when should one stop.

2.1.2.3. Spectral assignment. Unlike what might be commonly believed, assigning the paramagnetic spectra of lanthanide complexes can be relatively easy. The first approach comes with the question – is the Ln^{3+}/ligand system labile, i.e. does the ligand exchange between a free and a bound forms? If this is the case, we must go a step further: is the dynamic process fast, slow or intermediate on our NMR timescale?[4]

Fast exchange: one observes one set of resonances, whose position is concentration-dependent. In this case one can take advantage of a titration of the free ligand with the lanthanide, starting with very small aliquots of the latter, in order to follow the spreading of the signals. In fact, it is impossible to predict if a certain peak will move up- or down field and crossing may be the rule. This situation is often found with shift reagents reversibly binding to monodentate systems.

Slow exchange: two sets of resonances are more or less apparent, one for the free ligand, one for the complex. The very large paramagnetic shifts of most lanthanides from Eu^{3+} to Yb^{3+} (excluding Gd^{3+}) makes this situation rather common, especially when Ln^{3+} salts are mixed with polydentate ligands. Here it is most appropriate to try EXSY or saturation transfer experiments. One must find a mole ratio of Ln^{3+} and ligand such that both bound and free forms are populated. Then EXSY can be measured through the conventional NOESY sequence, by judiciously choosing the mixing time. The rule of the thumb to choose τ_{mix} close to an average T_1 does not help much and it may be wise to try a few quick runs with very different values. One must make sure that in the first spectrum one can recognise a reasonable number of paramagnetic resonances well above the noise. The ROESY version may be more difficult, because strong B_1 fields need to be applied in order to cover the very large spectral width. This may introduce significant artefacts and sample heating. Alternatively, one can use 1D saturation transfer by saturating the paramagnetic signals and observing the effect on the diamagnetic spectrum. Operating in the opposite configuration is not as effective, because the amplitude of the steady state signal detected is inversely proportional to the relaxation rate of the *observed* nucleus, which is naturally smaller. Moreover, the paramagnetic signals are usually more widely spread out, which reduces the risk of saturating two nuclei. The information derived through EXSY (or saturation transfer) may lead to the immediate assignment of the paramagnetic spectrum, provided that of the free form is known. The LIS is automatically measured.

Intermediate exchange is not easily amenable to any NMR analysis, because it is plagued by extensive line broadening. One should try and change temperature, solvent or, when possible, field.

Inert systems are those where the lanthanide is caught tightly by its ligand and no exchange between a free and a bound form is observed. This does *not* imply the absence of *any* dynamics, like conformational rearrangement or a labile coordination site, cases that will be discussed in some detail below. Assigning the paramagnetic spectrum is complicated by three factors: the shift is mostly due to paramagnetic interactions (contact and pseudocontact) and the usual correlations between environment and chemical shift do not hold; the line broadening erases most of the multiplet fine structure; efficient relaxation and wide spectral width prevent the successful use of many sequences based on complicated coherence transfer pathways. The simplest 2D experiments are usually the most useful and informative and one should generally avoid any sophistication: absolute value COSY, HETCOR or HMQC are among the most informative experiments, for assigning proton and carbon spectra. Heteronuclear correlation experiments are based on the good match between the total delay τ and the reciprocal of the scalar coupling. Indeed, maximum intensity is expected when $\tau = 1/J$. On the other hand, during this time, transverse relaxation can induce loss of magnetisation and using a shorter τ may be a wiser choice. In our experience, $\tau = 1$–5 ms can give good results. Fig. 2 contains a pictorial and simplified synthesis of the most relevant aspects of this section.

The pseudocontact shifts are determined by the position of the nucleus with respect to the lanthanide, which induces one to think that nearby nuclei will have similar δ^{pc}. This expectation may be completely false and misleading: consider that a pair of germinal protons on cyclene ring in Yb DOTA differ in resonance by more than 100 ppm and that for the other pair the δ^{pc} are opposite! [19].

There are, however, two distinct advantages when using paramagnetic NMR of Ln^{3+} complexes:

- the signals are usually spread and overlap is rare;
- the short relaxation time allows one to acquire at increased rate.

In any case, one should always measures the ^{1}H-T_1's by means of a simple inversion recovery: relaxation rates are very relevant pieces of information, which can be of some help in assigning the spectrum (spatially nearby nuclei have similar rates) and might be essential for structure refinement.

[4] A process is fast if $k \ll 2\pi\Delta\nu$ (Hz), which depends on the temperature, but also on the magnetic field and on the nucleus under observation. In fact the three dynamic regimes can apply for the same molecule at one temperature, but at different fields or for different nuclei.

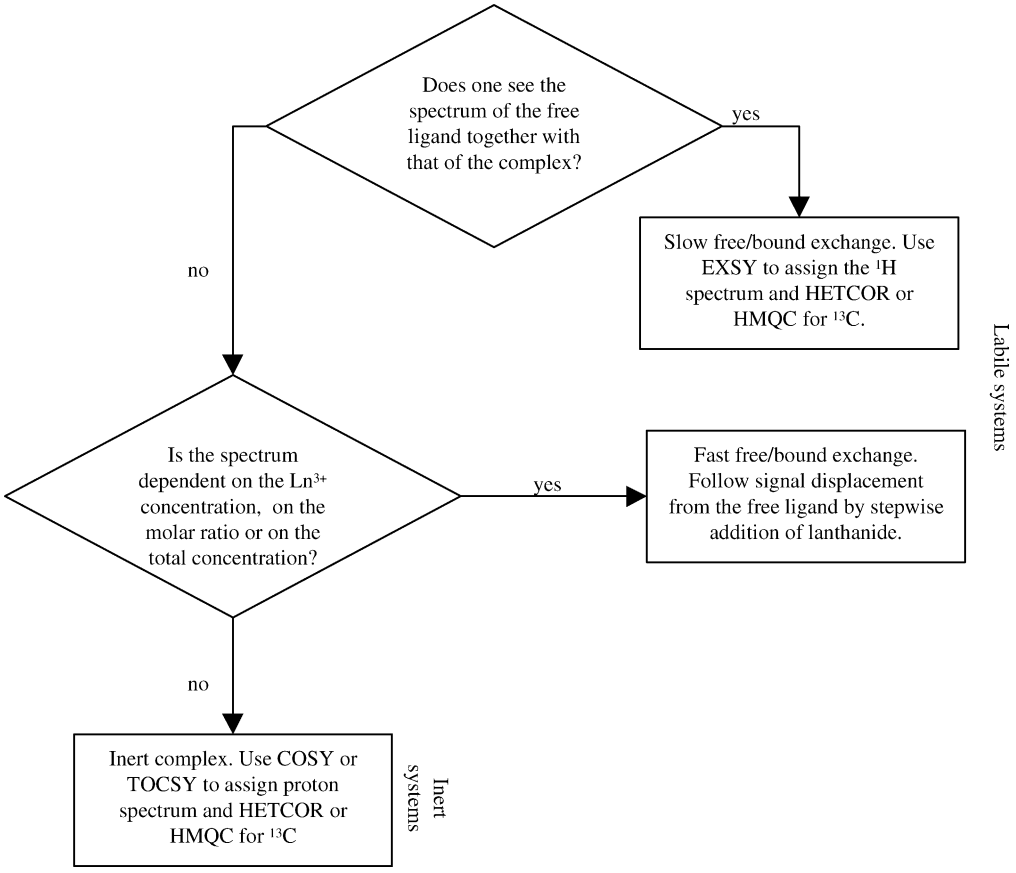

Fig. 2. Suggestions for assigning the spectra of paramagnetic complexes. Notice that: (1) success of EXSY is not guaranteed, since it depends on the exchange rate and on the relaxation time, as explained in the text; (2) one might have the simultaneous presence of the spectra of free and bound ligand (answer yes to the first question) also in the case of inert systems, in the presence of an excess of free ligand.

2.1.2.4. Choice of the lanthanide. When one is allowed to choose among the series, a few guidelines can help one to obtain the best spectroscopic response. As seen in Fig. 3, nuclei from Tb to Yb guarantee strongly shifted lines. The ratios δ^{pc}/δ^{c} and $\delta^{pc}/\Delta\nu$ provide a criterion to orient the choice: the larger the better, because the paramagnetic shift is least affected by contact and the line broadening is not too heavy. It is clear that Yb, Ce and Pr are the best choices in these respects. Samarium is not very good, instead, because δ^{pc} is almost vanishing.

When focussing on larger systems than those discussed in the present work, such as metalloproteins, it may be desirable to use Dy or Tb, which may significantly shift the resonances of distant nuclei. In this case, the contact interaction is unlikely to be a factor owing to the presumably large number of chemical bonds between nucleus and lanthanide.

Yb is confirmed a good system, also for its optical properties discussed below.

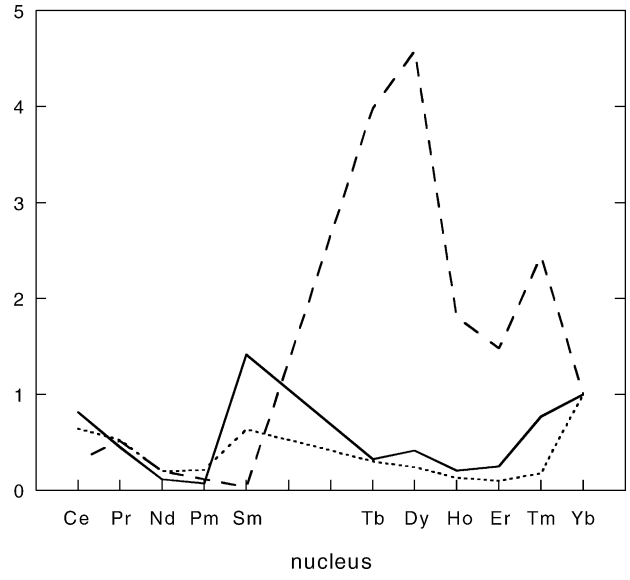

Fig. 3. Solid line: ratio between pseudocontact and contact shifts for a proton in a Ln^{3+} complex throughout the lanthanide series. Dotted line: ratio between proton δ^{pc} and linewidth $\Delta\nu$. Dashed line δ^{pc}. In all the three cases, the geometry of the arrangement, the magnetic anisotropy, and the external field can change the value (but not its relative trend), which is thus referred to Yb^{3+}.

2.2. Chiroptical spectroscopy

2.2.1. Selection rules

In 1980 Fred Richardson classified the f–f electronic transitions of Ln^{3+} systems with respect to their expected electric

Table 3
Richardson's classification of Ln^{3+} f–f electronic transitions [20]

Type	ΔS	ΔL	ΔJ
1	0	0	0, 1 ($J \neq 0 \neq J'$)
2	0	0	1 (J or $J' = 0$)
3	0	>0	0, 1 ($J \neq 0 \neq J'$)
4	0	>0	1 (J or $J' = 0$)
5	0	≥0	$2 \leq \lvert\Delta J\rvert \leq 6$ (J or $J' = 0$)
6	0	≥0	2, 4, or 6 (J or $J' = 0$)
7	0	≥0	3 or 5 (J or $J' = 0$)
8	0	≥0	0 ($J = J' = 0$)
9	>0	≥0	0, 1 ($J \neq 0 \neq J'$)
10	>0	≥0	1 (J or $J' = 0$)
11	>0	≥0	$2 \leq \lvert\Delta J\rvert \leq 6$ (J or $J' = 0$)
12	>0	≥0	2, 4, or 6 (J or $J' = 0$)
13	>0	≥0	3 or 5 (J or $J' = 0$)
14	>0	≥0	0 ($J = J' = 0$)

and magnetic dipole strengths and to the rotatory strength they acquire once the ions are embedded in a chiral environment [20]. First of all he divided all the possible transitions according to the change in ΔS, ΔL, or ΔJ into 14 classes as represented in Table 3.

Thereafter, he determined which are the transition types expected to yield: (A) the strongest electric dipole; (B) the rotatory power; (C) dissymmetry factor ($g = \Delta\varepsilon/\varepsilon$). These aspects play a fundamental role in the intensity detected through spectroscopy, as depicted in Table 4.

This means that for each lanthanide (except La, Gd and Lu) the transitions reported in Table 5 belong to the R I class and are expected to give rise to intense CD and CPL spectra.

Among these transitions, the nearest to the field commonly covered by commercial spectropolarimeters is the $^2F_{7/2} \rightarrow {}^2F_{5/2}$ of Yb^{3+}, which falls just at the beginning of near IR. On the contrary, many of the others are likely to interfere with chiroptical phenomena allied with vibrational spectroscopy. The transitions shown in Table 5 represent only a selection of the strongest rotatory strengths expected, which does not imply that other systems are not amenable to chiroptical investigation. In fact, there is a large manifold of investigations both connected to absorption and emission chiroptical spectroscopy of Ln^{3+} transitions.

Table 4
Classification scheme for electric dipole strength (A), rotatory strength (B), and dissymmetry factor (C) (the relative strengths are I > II > III > IV [20])

		Class	Transition types
(A)	Electric dipole strength (absorption and emission intensities)	E I	1, 3, 5, 6
		E II	9, 11, 12
		E III	2, 4, 7, 8
		E IV	10, 13, 14
(B)	Rotatory strength (CD and CPL intensities)	R I	1
		R II	2, 3, 5, 6, 9
		R III	4, 7, 8, 10, 11, 12
		R IV	13, 14
(C)	Dissymmetry factor	D I	2, 10
		D II	1, 4, 7, 8, 9, 13, 14
		D III	3, 5, 6, 11, 12

Table 5
Transitions belonging to the R I class [20]

Ion	Transition	Approximately trans. freq. (cm^{-1})	Approximately wavelength (nm)
Ce^{3+}	$^2F_{5/2} \rightarrow {}^2F_{7/2}$	2100	4760
Pr^{3+}	$^3H_4 \rightarrow {}^3H_5$	2150	4650
Nd^{3+}	$^4I_{9/2} \rightarrow {}^4I_{11/2}$	2000	5000
Pm^{3+}	$^5I_4 \rightarrow {}^5I_5$	1600	6250
Sm^{3+}	$^6H_{5/2} \rightarrow {}^6H_{7/2}$	1400	7140
Eu^{3+}	$^7F_1 \rightarrow {}^7F_2$	1100	9090
Tb^{3+}	$^7F_6 \rightarrow {}^7F_5$	2100	4760
Dy^{3+}	$^6H_{15/2} \rightarrow {}^6H_{13/2}$	3500	2860
Ho^{3+}	$^5I_8 \rightarrow {}^5I_7$	5000	2000
Er^{3+}	$^4I_{15/2} \rightarrow {}^4I_{13/2}$	6400	1560
Tm^{3+}	$^3H_6 \rightarrow {}^4H_5$	5800	1720
Yb^{3+}	$^2F_{7/2} \rightarrow {}^2F_{5/2}$	10000	1000

2.2.2. *Absorption and emission chiroptical spectroscopy: CD and CPL*

Chiroptical techniques are a powerful tool for investigating chiral molecules for several reasons. In the first place, circular dichroism and circularly polarised luminescence, CD and CPL, provide *unique* spectroscopic data sensitive to the absolute configuration and the enantiomeric composition of a substrate not depending on diastereomeric interactions. Moreover, there is a neat increase in sensitivity to the chemical environment of a given chromophore with respect to the non-polarised (sometimes defined *isotropic*) absorption or emission phenomena. Finally, the fact that the chiroptical bands can have different signs often implies spectra with improved resolution. In fact, two partially overlapping bands of the same sign tend to merge and to appear as one absorption peak, while if they have opposite sign, there is a cancellation effect, which makes the two components clearly distinguishable. In a completely different context, this effect is well known: for example to those accustomed to the antiphase doublets of DQF-COSY spectra, where even small active J-couplings can become apparent, while they provide no splitting in the in-phase 1D spectrum.

The $^2F_{7/2} \rightarrow {}^2F_{5/2}$ of Yb^{3+} is in fact a manifold of transitions centred around 980 nm: in a crystal field the lower lying state $^2F_{7/2}$ splits into four sublevels, characterised by the M_J components ($M_J = \pm 7/2; \pm 5/2; \pm 3/2; \pm 1/2$), while the upper state $^2F_{5/2}$ splits into three ($M_J = \pm 5/2; \pm 3/2; \pm 1/2$). If the crystal field splitting of the ground state is comparable to – or smaller than – kT at room temperature (which is indeed the case in the examples reported so far), the sublevels are populated according to a Boltzmann distribution and in principle up to 12 electronic transitions can be observed (starting from each M_J component of $^2F_{7/2}$ and aiming at the three sublevels of $^2F_{5/2}$), following the schematic representation of Fig. 4. On lowering the temperature, the relative population of the ground sublevel approaches unity and only the transitions starting from it survive.

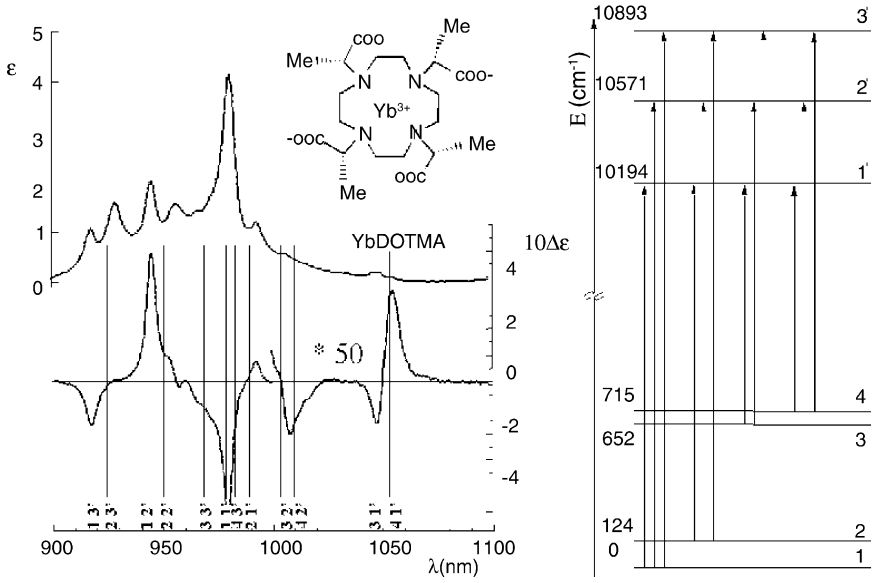

Fig. 4. Crystal field splitting and hot bands in Yb DOTMA, a chiral ytterbium complex. On the left: NIR absorption and CD spectrum, where the individual transitions have been assigned; on the right: energy splitting of the ground ($^2F_{7/2}$) and excited ($^2F_{5/2}$) electronic states [21].

This has been used as a tool for a tentative assignment of the energies of the electronic sublevels of Yb in YbDOTMA. One can perform a quantitative evaluation of the rotational strength $R(T)$ of the individual dichroic bands as a function of temperature, and one expects that each transition is characterised by an intrinsic rotational strength R', multiplied by a Boltzmann factor $b(T)$:

$$R(T) = R'b(T) \tag{30}$$

From the spectrum at low temperature (−80 °C), shown in Fig. 5, one can recognise the two energy splittings of the upper level, $^2F_{5/2}$, then these data are used to find the same spacing of lines at room temperature. The values tentatively found are shown in Fig. 4 [21].

Almost all lanthanides have fluorescent transitions and can give rise to interesting emission and CPL spectra. In many applications, this is made possible through the introduction of an organic chromophore capturing UV radiation and sensitising the Ln^{3+}, which in turn gives rise to luminescence in Vis or NIR. The overall process is dominated by an intra or an intermolecular energy transfer [22,23]. This situation has been used to monitor the environment of both the lanthanide and the organic moiety. Notably, it served as a sensor for pH [24], pO_2 [25] anions [26], alkali cations [27], and for interaction with nucleic acids [28]. To this end, the most widely used systems are Tb, Eu, more rarely Er, Yb, and the others.

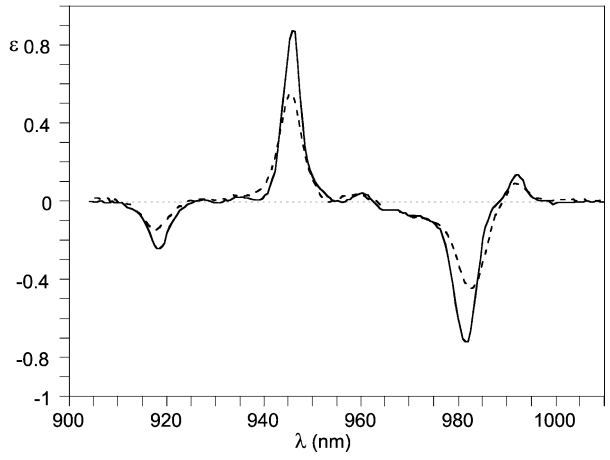

Fig. 5. Temperature dependent NIR–CD spectra of YbDOTMA. Continuous line 298 K; dashed line 218 K [21].

A considerable amount of work has been invested to determine the energy levels involved in the transition, exploiting CD and emission spectroscopy. This was done primarily by Richardson's group [29], and will not be further reviewed here.

Nowadays many commercial CD instruments offer wavelength extension to 1100 nm, in the near infrared as an optional device. This is completely adequate to observe Yb, Tm, Er, Dy, and Nd NIR-transitions. We work with a home-built tandem detector Si/InGaAs, on an old Jasco J200D, equipped with a halogen lamp [30]. The large rotational strength allied with the $^2F_{7/2} \rightarrow {}^2F_{5/2}$ of Yb^{3+} in a chiral environment makes the detection of CD spectra particularly easy, and often simpler than the accurate measurement of the absorption itself. This is notably true especially when water or an alcohol is the solvent, because between 900 and 1100 nm there is an O–H stretching overtone. Owing to its small extinction coefficient it does not interfere with CD (the anisotropy factor $\Delta A/A$ remains larger than 10^{-3}), but may require repeated accumulation to obtain satisfactory accuracy in absorption. Things are much easier when heavy water is used instead of H_2O.

Owing to the small absorptions allied with the electric-dipole forbidden f–f transitions of Ln^{3+}, CPL may require laser excitation, especially for complexes lacking aromatic

groups (see the description of antenna systems below in Section 3.3).

2.3. Connection between optical spectra and magnetic properties

Lanthanide 4f orbitals are weakly affected by the donor atoms in the environment, because they are deeply buried under the 5d shell. Consequently, unlike transition metals, the crystal field splitting is usually small, and constitutes a minor perturbation to spin–orbit coupling. This means that the centre of gravity of all the state-to-state transitions is, to a first approximation, independent of the ligands, which determines, instead, the spread of the lines. With reference to Fig. 4 above, the separation between the sublevels of the ground electronic state of Yb^{3+} in YbDOTMA is comparable to kT (at room temperature, $kT \approx 200\,cm^{-1}$), which justifies the appearance of *hot bands*, described in the previous section. The appearance of the optical spectrum (position and intensity of the absorption, emission, and dichroic bands) can be related to the crystal field parameters, expressed as spherical harmonic components B_q^k, where $-k \leq q \leq k$ and $0 \leq k \leq 6$ [31]. The crystal field parameters are also responsible for the magnetic properties of the Ln^{3+} ions and a relation between optical and NMR spectra has been sought through Bleaney's theory [8]. This treatment suffers from one major limitation: the assumption that the crystal field splitting is small compared to kT, which is likely to be violated by many systems, notably by Yb^{3+}, as discussed above. Mironov et al. proposed a more complete approach and calculated the magnetic anisotropy for a variety of systems, as a function of the ligand geometry [9].

Bleaney's theory predicted a definite trend for the δ^{pc} through the Ln^{3+} series and this was the basis for several investigations [32]. Interestingly, in a pioneering report of a scan of δ^{pc} throughout the series, Horrocks and Sipe [33] found a trend, which very closely parallels Bleaney's [8] prediction and the very recent Bertini validation [34].

Parker et al. made an attempt directly to relate the appearance of optical and NMR spectra, thus bypassing any explicit reference to crystal field parameters, which are modulated by the axial ligand [35]. This will be discussed in the following section.

2.3.1. The role of the axial ligand

Many functional lanthanide complexes share a common feature: more or less inert binding to an organic ligand and one or more labile sites, where molecules containing donor groups and atoms can be temporarily hosted. By doing so, the chemical and spectroscopic properties of this molecule may be drastically modified. Three examples will clarify the matter.

Shift reagents, where the guest molecule falls under the influence of the large magnetic anisotropy of Ln^{3+}; this possibly induces large shift differences and resolves peak overlap. The organic ligand in the first place makes the lanthanide soluble in apolar media. Moreover, when it is chiral it may differentiate isochronous enantiotopic nuclei in the guest.

Magnetic resonance contrast agents are usually complexes of Gd^{3+} exploiting the very efficient nuclear relaxation experienced by water molecules coordinating to the lanthanide. The organic ligand must ensure sufficient stability to prevent release of the lanthanide in the living organism. Secondly, it modulates the properties of the system, for example the rotational correlation time, the exchange rate or, in more sophisticated application, it lends itself to interaction with specific target biomolecules.

Lanthanide-based catalysts for stereoselective reactions are often postulated to polarise the substrate, through a Lewis acid (the Ln^{3+}) – Lewis base interaction, while the ligand provides the chiral environment responsible for a definite reaction stereochemistry.

In all these cases it is essential that many guest molecules come in contact with the Ln^{3+}, i.e. that the axial coordination site is exchangeable.

In the recent past, we have examined this process from the point of view of crystal field parameters, finding that the axial ligand plays a very large role in determining the magnetic anisotropy of Yb^{3+} [36]. The ^1H spectrum of the organic ligand in $[Yb(DOTAMNp)]^{3+}$ (see Fig. 6) changes dramatically when DMSO is added to a CD_3CN solution. Because both complexes are axially symmetrical, the

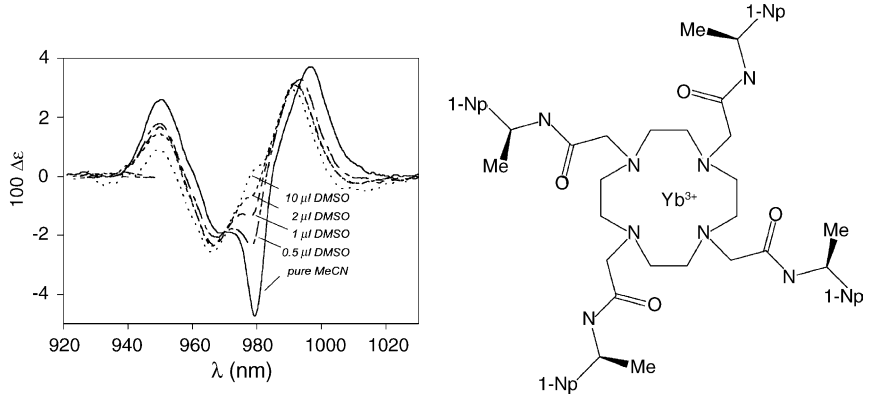

Fig. 6. NIR–CD spectrum of $[Yb(DOTAMNp)]^{3+}$ as a function of DMSO added to a CH_3CN solution [36].

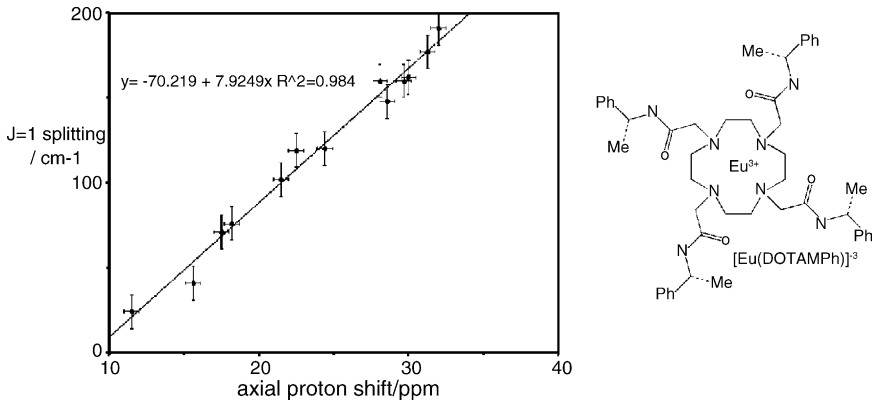

Fig. 7. Correlation of the ^{1}H NMR shift of the most shifted axial ring proton, in $[Eu(DOTAMPh)]^{3+}$ with the separation of the A_2–A_1 and E–A_1 optical transitions in the $\Delta J = 1$ emission band ($\pm 10\,cm^{-1}$) for 13 different O and N axial donors (295 K, 1 mM complex).

McConnel–Robertson equation (20) is valid and, provided no structural rearrangement takes place between free and bound forms, the spectra can be fully accounted for by one parameter D, which is a function of the axial ligand strength. According to Bleaney, it is directly proportional to the sole crystal field parameter B_0^2.[5] In fact, two different effects concur in determining this dependence. The increasing (negative) charge or polarisability of the ligand reflects directly in B_0^2, moreover if there is an equilibrium between a capped and a non-capped form, this is likely to be displaced more in favour of the former with stronger donors. Interestingly, the modification of the ^{1}H NMR is parallel to that of the NIR–CD spectrum, as demonstrated in Fig. 6.

Moving from this observation, Parker and Dickins argued that the optical and NMR spectra of the chiral complex $[Eu(DOTAMPh)]^{3+}$ of Fig. 7 can be directly related, avoiding explicit reference to the crystal field parameters [35]. Babushkina et al. [32] had reported that the sublevels of the states $^7F_1$ and $^5D_0$ of Eu^{3+} are split only by second order harmonics, which – in an axial system – reduce to B_0^2, also responsible for the D parameter of Eq. (20), according to Bleaney [8]. The value of the observed shift for the axial proton in DOTA-like systems is a good measure of D, provided contact interaction can be neglected. The straight line of Fig. 7 is a demonstration of the validity of this approach.

The same authors related the amplitude of the NIR–CD spectrum of $[Yb(DOTAMPh)]^{3+}$ at 975 nm with the axial proton shift.

3. Applications

3.1. C_2-symmetric complexes

This class of symmetry is rather well represented for catalytically active compounds, because it conjugates two important features: leaving the metal centre relatively accessible to reactants and reducing the number of non-equivalent reaction pathways [37]. Unfortunately, the solution structure of many such derivatives has not yet been investigated, and we hope that in the near future more reports on this subject will be published. Several reasons may prevent widespread geometry determination of Ln^{3+} complexes. In the first place the lack of general software suitable for the analysis of δ^{pc} and relaxation rates of small molecules, as outlined above. Secondly, the high degree of fluxionality often exhibited by these complexes, at least on some coordination sites. Very recently, we became interested in the analysis of a chiral complex based on a neutral hexaazamacrocycle, obtained by condensation of diformylpyridine and *trans*-diaminocyclohexane, shown in Fig. 8 [38,39]. This system exhibits D_2 symmetry in the solid state and in solution. Two NO_3^- are axially bound and a further nitrate is in the outer coordination sphere.

The solution structure has been confirmed to be practically identical to the X-ray geometry, by analysis of the δ^{pc}. Indeed, lacking axial symmetry, this complex must exhibit a certain degree of anisotropy of the magnetic susceptibility tensor and the full Eq. (18) has to be employed. The D_2 symmetry ensures that the principal axes of the inertia and magnetic tensors coincide, i.e. that the principal components of $\boldsymbol{\chi}$ are to be found along the three orthogonal C_2 axes. This greatly simplifies the task, because the geometrical factors are immediately defined in Eq. (19). When a salt of a different anion is added to the solution, the NMR spectrum undergoes profound changes, which reflect once more the sensitivity of the crystal field parameters to the donor strength of the axial ligands. Unlike the previous discussion in Section 2.3.1, in this case, two D parameters are relevant, and both – possibly to a different extent – show the consequence of the anion change. Moreover, as clearly seen in Fig. 8, there are two axial sites, one above, one below the macrocycle pseudoplane. This means that the anion exchange can take place stepwise and that species with C_2 symmetry can be formed, where the axial ligands are different: assuming one titrates the complex $Yb\mathbf{L}A_2$ with the anion B^-, the two equilibria ought to be

[5] Following Mironov instead, the dependence is not as simple [9]. For the present argument, however, this has no practical effect, because we avoid any precise reference to the nature of the crystal field terms.

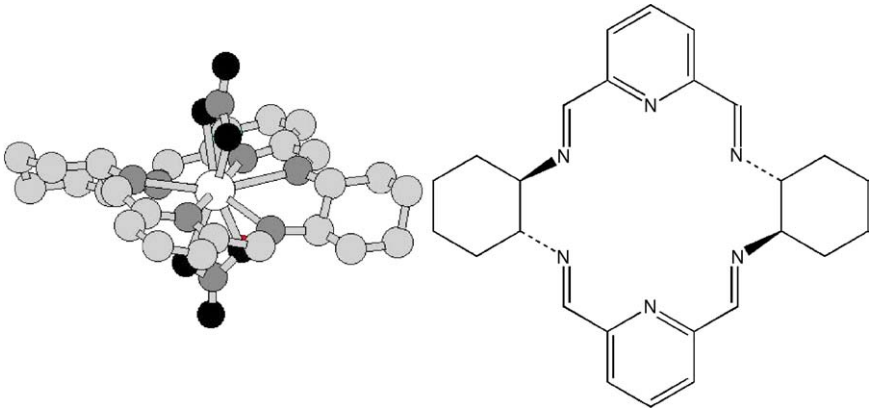

Fig. 8. Structure of the hexaazamacrocyclic L*Tm$(NO_3)_3$ complex. The chiral ligand L* is depicted on the right [38a].

considered

$$\mathrm{YbLA_2} \underset{\mathrm{A^-}}{\overset{\mathrm{B^-}}{\rightleftarrows}} \mathrm{YbLAB} \underset{\mathrm{A^-}}{\overset{\mathrm{B^-}}{\rightleftarrows}} \mathrm{YbLB_2} \quad (31)$$

This is readily apparent in the ^{1}H NMR spectrum because the systems Yb**L**A_2 and Yb**L**B_2 have D_2 symmetry, and only eight resonances are to be expected, owing to magnetic proton equivalence, while in the case of the lower C_2 symmetry species Yb**L**AB 15 different shifts are envisaged.

The situation may be complicated by the dynamic regime of the exchange processes. Let us focus on the first step of Eq. (31) above. If it is slow, during the course of the titration one observes the superposition of the spectra of the two species. EXSY experiments can readily correlate the proton shifts of **L**. The δ^{pc} can be ascribed to the pure Yb**L**A_2 and to the pure Yb**L**AB. If the exchange is fast, instead, in a generic point of the titration, the spectrum displays lines whose shift do not represent any pure species, but fall at weighted averages of the limiting cases preventing a straightforward analysis. Care must be taken to extract the δ^{pc} sufficiently near to the case where only one species is present. The situation can be clarified, taking advantage of an "intrinsically fast" spectroscopy, like NIR–CD. Indeed, for the timescale of optical spectroscopies practically all exchange processes appear slow and the spectra are the superposition of contributions from the various species. The sensitivity of this spectroscopy to the axial ligand was already discussed for symmetric complexes in Section 2.3.1 and is further confirmed in Fig. 9.

The analysis of the δ^{pc} demonstrates that:

- The geometry of the macrocycle is insensitive (within the accuracy limits of the method) to the axial ligand exchange.
- The magnetic susceptibility is strongly dependent on the axial ligand.
- The results of the analysis for the systems of lower symmetry are depicted in Fig. 10. The graphical representation of the magnetic susceptibility tensor gives an immediate feeling that it is grossly approximated by a prolate ellipsoid, with the main axis roughly directed between the two cyclohexyldiamine nitrogen atoms.

Furthermore, by NIR–CD, one can establish a spectroscopic series for the ligands investigated:

$$\mathrm{PhSO_3^-} < \mathrm{Cl^-} < \mathrm{NO_3^-} < \mathrm{AcO^-} < \text{phenylphosphate}^{-2},\ \text{diphenylphosphate}^-$$

3.2. C_3-symmetric complexes

A family of enantioselective catalysts belongs to this class, obtained by reacting an alkali metal binaphthoate with a lanthanide salt. These complexes are often known as Shibasaki's catalysts [40]. Several preparations have been described in the literature, the most effective ones starting from the readily soluble Ln(iPrO)$_3$ or Ln(TfO)$_3$, although, also the chlorides may provide good results. The X-ray structures of these

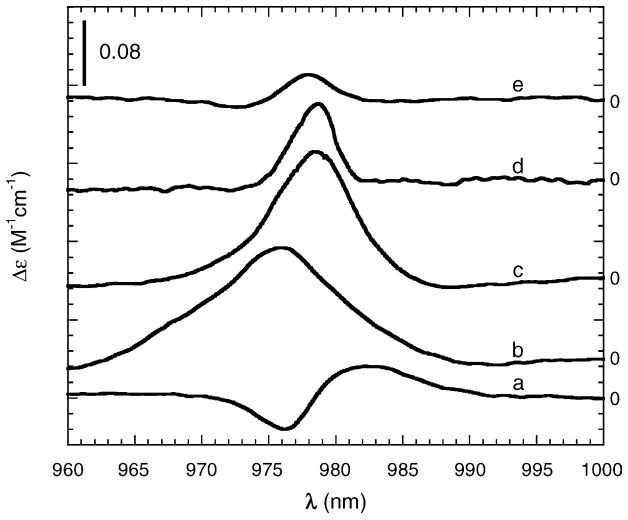

Fig. 9. NIR–CD spectrum of: (a) [YbLCl$_3$]·2H$_2$O (6.52 mM) in CHCl$_3$/MeOH 2:1, (b) [YbL$(NO_3)_2(NO_3)$] 6.10 mM in CHCl$_3$/MeOH 2:1, (c) [YbL$(NO_3)_2(NO_3)$] 3.13 mM in CHCl$_3$/MeOH 2:1 after adding of 2.4 equiv. of AcONa (130.00 mM), (d) [YbLCl$_3$] 2.67 mM in CHCl$_3$/MeOH 2:1 after adding of 3.5 equiv. of PPNa$_2$ (57.47 mM), (e) [YbL$(NO_3)_2(NO_3)$] 3.50 mM in CHCl$_3$/MeOH 2:1 after adding of 2.5 equiv. of DPPNa (24.68 mM) [38].

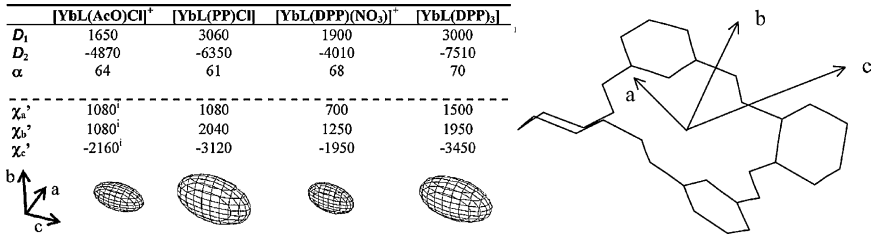

	[YbL(AcO)Cl]$^+$	[YbL(PP)Cl]	[YbL(DPP)(NO$_3$)]$^+$	[YbL(DPP)$_3$]
D_1	1650	3060	1900	3000
D_2	-4870	-6350	-4010	-7510
α	64	61	68	70
χ_a'	1080[f]	1080	700	1500
χ_b'	1080[i]	2040	1250	1950
χ_c'	-2160[i]	-3120	-1950	-3450

Fig. 10. Results of the analysis of the δ^{pc} for a series of ternary adducts of C_2 symmetry, with reference to the hexaazamacrocyclic ligand L*. Calculated values of D_1, D_2 (ppm Å^3, error within 10–20%) and α ($\pm 5^\circ$) following Eq. (19), and of the components of the magnetic susceptibility tensor in its principal axes system (a, b, c) indicated on the right. In the bottom line, the magnetic susceptibility ellipsoids are also depicted [38].

compounds have been exhaustively reviewed by Aspinall [41].

The main feature is that in the solid state, they give rise to an approximate trigonal antiprismatic coordination polyhedron, shown in Fig. 11 [42].

In the first part of the series, from La to Eu, a water molecule occupies an axial position, capping the antiprism. From Eu to Yb, non-capped complexes are stable. Thus, europium can give rise to both 6 and 7 coordinated species. The polyhedron may be conically distorted, with the upper triangle defined by the oxygen atoms slightly wider than the lower. For the early lanthanides, this may appear a consequence of the capping water ligand, but such a feature is preserved at least for some systems throughout the series independently of the occupancy of the axial site. A notable exception is provided by YbLi$_3$[(*S*)-BINOL]$_3$, which displays D_3 symmetry even in the solid state. The ^{1}H and ^{13}C NMR spectra of YbNa$_3$[(*S*)-BINOL]$_3$ immediately reveal that the six naphthalene units are equivalent at all temperatures, down to 173 K, where no decoalescence occur. Accordingly, the system in THF solution must be considered truly symmetrical and not only dynamically so. A detailed analysis of the hyperfine shifts was performed first by Aspinall [43], assuming the solid state structure. This study demonstrated that this geometry is substantially conserved in solution. More recently, we reanalysed the problem, without making assumptions, with the aid of the program PERSEUS described in Section 2.1.2: we varied the dihedral angle of a binaphthol unit, together with the Yb coordinates and the magnetic susceptibility tensor components, in a global fitting of the ^{1}H-T_1 and δ^{pc} and of the ^{13}C δ^{pc}. The result was a fragment of the complex, with Yb^{3+} defining the coordination polyhedron centre, and the main axis of the symmetric susceptibility coincident with the C_3 axis. The whole geometry is obtained by constructing the symmetric images of the binaphthol ligand. Therefore, this structure is built exclusively on the basis of NMR constraints and does not rely upon previous knowledge (apart from a reasonable geometry of the naphthol moiety). Water is not bound to the complex in THF solution, as demonstrated by the fact that H_2O resonates at the usual frequency and that no low field signal can be assigned to axial ligation. This is taken as a good hint that YbM$_3$[(*S*)-BINOL]$_3$ (at least for M = K, Na) cannot expand the coordination number, probably on account of the small ionic radius of Yb^{3+} and of the bulk exerted by the ligand. In the X-ray structure, the angle O–Yb–O is smaller than 120° from the wider rim, smaller than 110° from the narrower rim. In the symmetrical solution structure, this angle is anyway smaller than 120°.

These compounds are extremely interesting also from the point of view of chiroptical spectroscopy: they lend themselves to simultaneous examination of ligand-centred transitions in the UV and of metal-centred NIR–CD. Naphthalene

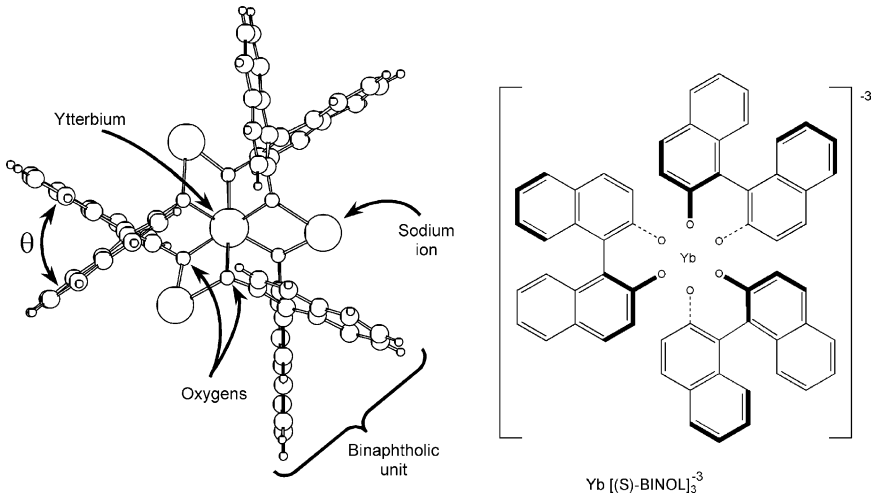

Fig. 11. X-ray structure of YbNa$_3$[(*S*)-BINOL]$_3$ viewed almost along the C_3 axis [42].

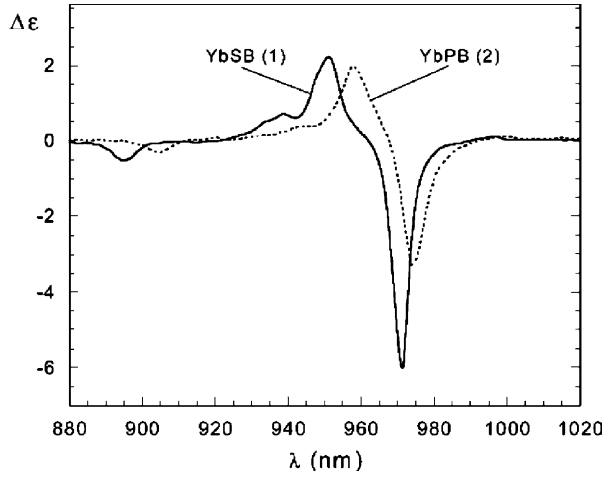

Fig. 12. NIR–CD spectra of $YbM_3[(S)\text{-BINOL}]_3$ with M = Na (continuous line) and M = K (dotted line).

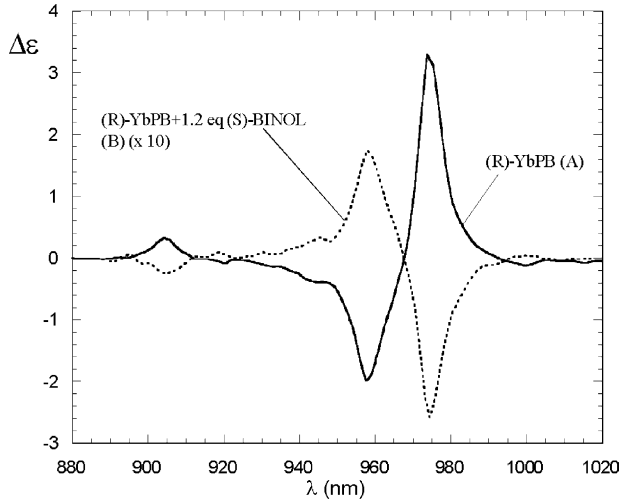

Fig. 13. NIR–CD spectrum of $YbK_3[(R)\text{-BINOL}]_3$ (indicated as (*R*)-YbPB) before (continuous line), and after (dotted line) the addition of a molar excess of (*S*)-BINOL [45].

is a very powerful organic chromophore with a well described UV spectrum, largely dominated by the ^1B_b transition around 220 nm and polarised parallel to the long axis. In chiral non-racemic compounds, this may give rise to intense CD spectra, which reflect the overall molecular stereochemistry [44]. By using the DeVoe approach to the quantitative interpretation of the CD spectra, the relative orientation of naphthol moieties can be investigated. In the case of $YbM_3[(S)\text{-BINOL}]_3$, this method confirms the solution structure determined through the NMR analysis [42].

The case of $YbM_3[(S)\text{-BINOL}]_3$ elucidates at least two very important points, which will hopefully help the rational approach to understanding chiroptical spectroscopy of Yb^{3+}.

In the first place, the coordination polyhedron of the molecule is achiral (it has D_{3d} symmetry), which implies that the charged oxygen atoms cannot be held responsible for the observed Cotton effects. The optical activity must thus be ascribed to a coupling with the organic backbone.

Secondly, there is a remarkable difference in the spectral width spanned by the potassium and the sodium derivative (see Fig. 12). This fits nicely with the NMR spectra, which are characterised by $D = 645$ for M = K and $D = 1770$ for M = Na.

EXSY spectra recorded after adding an excess of free ligand demonstrate that the Yb^{3+}–BINOL bond is labile, which, together with the observation that ytterbium remains six-coordinated, even in the presence of water, is a good indication that any catalytic mechanism involving this complex may involve a ligand-to-substrate exchange [45].

The observation of the lability of bound BINOL suggests that in the presence of the free ligand of opposite configuration, one may prepare directly in solution diastereomeric complexes such as $YbM_3[(S)\text{-BINOL}]_2[(R)\text{-BINOL}]$ and possibly even invert the configuration of the whole complex. This is what is indeed observed.

By simply mixing $YbK_3[(R)\text{-BINOL}]_3$ with (*S*)-BINOL, one can detect the NMR signals of a small amount of the heterochiral complexes. Similar systems had been reported previously only as a consequence of the reaction of a Ln^{3+} salt with racemic binaphthol and the dynamic process of ligand shuffling had not been revealed [43]. The amount of heterochiral complex at least when M = K remains well below 10%, witnessing a strong preference for the homochiral species, which appears to be more stable. When a molar excess of (*R*)-BINOL is added, one might expect a complete chirality inversion, which is indeed demonstrated through the NIR–CD spectra of Fig. 13.

Another class of C_3-symmetric molecules, which have been thoroughly investigated by means of NMR is provided by helicates. These are self-assembled systems, where three ditopic ligands are held together in the form of a twisted bundle by metal ions. These systems are among the best characterised for the separation of contact and pseudocontact contributions. The name helicate itself strongly calls for chirality, but unfortunately most of these complexes are prepared as racemates. Nice examples of non-racemic systems are those recently described by Horrocks et al., who took advantage of stereodefined centres introduced on the ligand, reflected in a precise preference for one sense of helical twist [46].

Molecular mechanics calculations indicate that the ΔΔ conformation should be preferred, as depicted in Fig. 14. Indeed the CD spectrum shown in Fig. 14, clearly demonstrates that Nd^{3+} is embedded in a chiral environment. Unfortunately it is weak and does not allow any safe correlation to those of Fig. 21 below.

The induction of chirality from the carbon backbone to the aggregate in helicates may be incomplete and may lead to the formation of diastereomers (combining the stereogenic elements on the ligand with the two helical twists). On the contrary, in a recent report Piguet et al. prepared enantiopure helicates containing d and f metals, and devoid of chiral centres on the ligand, by exploiting the stereochemical inertness of Cr complexes [47]. They characterised completely

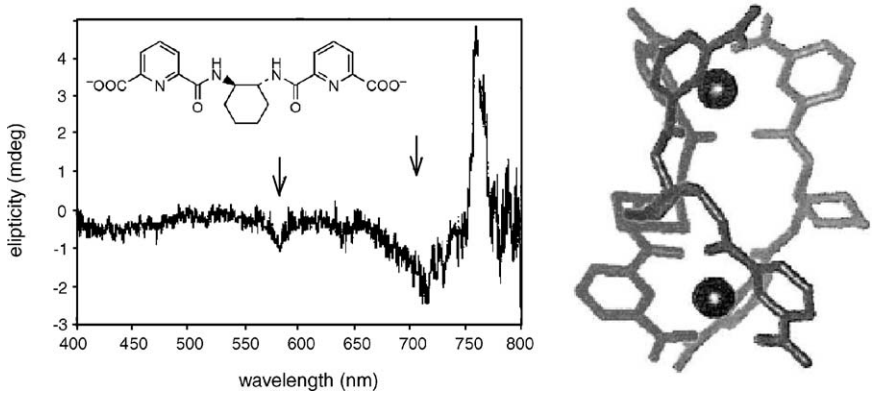

Fig. 14. Vis–CD spectrum of the neodymium helicate Nd_2 [dpa-chxn-*R*,*R*]$_3$. The chiral ligand is represented in the insert and the structure of the complex is shown on the right [46].

the Eu–Cr derivative, providing CD and CPL spectra, which feature high luminescence dissymmetry factors. By doing so, they demonstrated that helicity is an efficient tool for generating high CPL signals.

3.3. C_4-symmetric complexes

The derivatives of DOTA, based on tetra *N*-substituted cyclene macrocycles constitute the best characterised class of Ln^{3+} compounds [48]. This is largely due to the possible implications and use of the Gd^{3+} complexes as MRI contrast agents. The eight-fold coordination of DOTA provides a tight cage, ensuring stability and low toxicity. The very high formation constant, however, does not imply a complete kinetic inertness, on the contrary. The axial position of many systems is labile, which is determinant in their role in MRI: the exchange rate of water molecules for Gd DOTA$^-$ is about 4×10^6 s^{-1}, ensuring high relaxivity [49]. Moreover, the cage itself undergoes very relevant dynamic conformational processes, which are best explained in the prototype system LnDOTA$^-$ (see Fig. 15). Owing to steric interference between the acetate side arms, the complex must adopt an ordered conformation, where all the arms bend on the same side, giving rise to a more or less twisted tetragonal prism.

The four N- and the four O-atoms constitute the top and the bottom squares and the distortion is conveniently described through the tilt angle φ, between them: $\varphi = 0^\circ$ is a perfect prism, $\varphi = 45^\circ$ is a square antiprism. This leads to an overall chirality of the coordination cage, which is defined Δ or Λ, as depicted in Figs. 15 and 16.

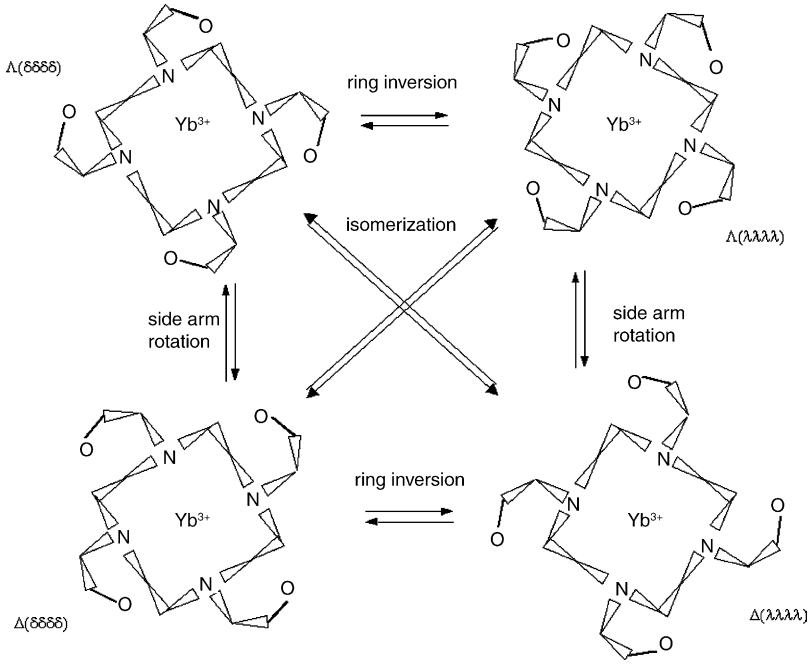

Fig. 15. Stereochemistry of Yb DOTA$^-$. The species across the diagonals are enantiomers, while between top and bottom lines, and left and right columns there is a conformational diastereomer relation.

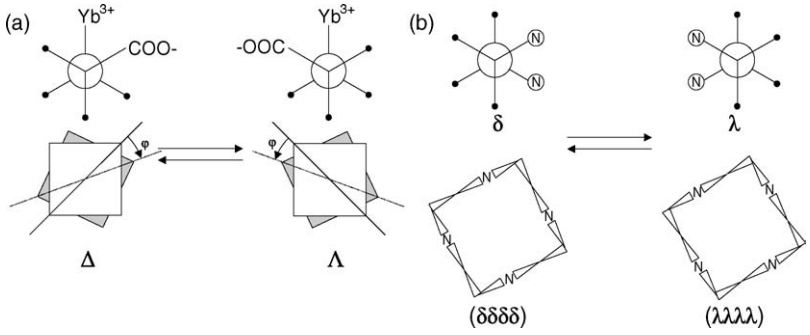

Fig. 16. (a) Equilibria between the Δ and Λ chirality of the coordination cage in Yb DOTA analogues. On the top line, the Newmann projection along the C–N bond is depicted; on the bottom, the overlapped squares represent the two planes, one defined by the four nitrogen atoms, one of the oxygen atoms (at the corners); (b) equilibria between the δ and λ forms of the cyclene ring. In the top line the two *gauche* conformation of a cyclene ethylenic bond are depicted; the bottom line represents through wedges the enantiomeric [3333] conformations of cyclene.

Neither limiting case has been observed so far in the crystal structures and most known geometries cluster around two values: $\varphi = 15^\circ$ and 30°. This means that the coordination polyhedron is itself chiral. In the absence of further stereodefined chiral elements, the two enantiomeric conformations must be equally populated at the equilibrium. Owing to the relatively efficient fluxionality usually displayed by lanthanides, the equilibration is ensured at room temperature.

Another element of conformational chirality is embedded the macrocycle: the most stable [3333] conformation of cyclododecane [50] admits two enantiomers, distinguished by the g^+ or g^- arrangement of CH_2–CH_2 bonds, as depicted in Fig. 16. A common notation for these two enantiomers is (δδδδ) and (λλλλ) for g^+ or g^-, respectively.

The two chiral elements recognised so far combine to yield four stereoisomers: the enantiomer pairs Λ(δδδδ)/Δ(λλλλ) and Δ(δδδδ)/Λ(λλλλ), which are in a diastereomeric relationship with each other. The former gives rise to a quasi-antiprismatic conformation, often referred to as SA (square antiprism), whereas the latter is definitely a twisted square antiprism (TSA). All $LnDOTA^-$ in solution display an equilibrium between these two forms, with relative populations varying along the series.[6] The interconversion between the two diastereomers SA and TSA may proceed through the concerted rotation of the four side arms (e.g. Λ(δδδδ) → Δ(δδδδ)) or through the inversion of the macrocycle (e.g. Λ(δδδδ) → Λ(λλλλ)). Of course these two operations correspond to two completely different pathways, endowed for example with different activation parameters, but they join a given substrate with two products that are enantiomers and thus non-distinguished by NMR.

The fact that the two forms Λ(δδδδ) and Λ(λλλλ) differ only by the cyclene inversion immediately explains a feature, which until recently was largely overlooked in the literature: the geometrical factors of the two diastereomeric forms of DOTA derivatives are practically identical and, as a consequence, their ^{1}H NMR spectra are proportional.[7] This is clearly seen for Yb $DOTMA^-$ in Fig. 17 [51,52], and demonstrates that the attempts to assign the spectra to one of two forms (SA or TSA) on the basis of the δ^{pc} analysis only are vain.

Mironov et al. [9] provided calculations for the dependence of the magnetic anisotropy parameter D on the twist angle φ and demonstrated that for Yb^{3+} one should expect $D(SA) > D(TSA)$. It should be observed that this observation is in contrast with Bleaney's theory [8], because the crystal field parameter B_0^2 – to which D is proportional– is independent of the twist angle of a distorted square prism. Indeed, the ^{1}H NMR spectra for Yb DOTA-analogues displaying the two diastereomeric conformations span very different spectral widths, confirming the validity of Mironov's approach. On top of this factor, there is the variable axial coordination often exhibited by the two conformers. The SA conformation of Yb $DOTA^-$ is much more exposed to the solvent than the TSA: this can be conveniently measured through the angle O–Yb–O (sometimes called bite angle [53]) relative to two opposite carboxylates for SA it is 155°, for a TSA it reduces to 133°. The effect of the axial ligand was already discussed in Section 2.3.1, where its profound influence on D was demonstrated.

Thus, at least two factors participate in determining the value of the magnetic anisotropy observed in LnDOTA derivatives.

An important consequence of axial dynamics, which has not yet found adequate space in the literature is its effect on NMR linewidths and T_1's. In Yb compounds completely devoid of any axial ligand, one observes comparatively narrow resonances for most protons, in agreement with, or narrower, than the values reported in the last line of Table 1. On the contrary, systems featuring axial dynamics are characterised by more or less pronounced line broadening. A remarkable

[6] The literature in the field is dominated by the descriptors *M* and *m* for SA and TSA, respectively, with reference to the major and minor forms of $YbDOTA^-$. We believe that this nomenclature is very confusing and that it should be avoided.

[7] Properly speaking, this is true only for the pseudocontact shifts, because neither δ^c nor δ^{dia} are proportional to the geometrical factors. The large values usually found for the magnetic anisotropy in these systems, however makes these contributions practically negligible.

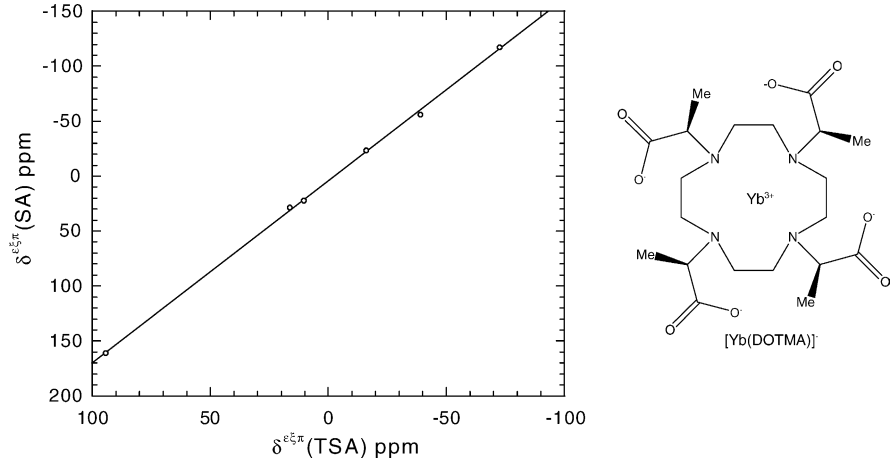

Fig. 17. Correlation plot between the experimental values δ^{exp} of the two forms of Yb DOTMA in D_2O [51].

case is offered by Yb DOTMA$^-$, where the two isomers give rise to spectra with differential line broadening, as if they responded to completely different correlation times, as shown in Table 6.

Interestingly this same situation can be found also for YbDOTA$^-$, where the linewidths difference between TSA and SA is reverted. Such a paradox may be clarified, considering that both isomers are subject to a hydration–dehydration equilibrium, in analogy with what described for LnDOTA$^-$ [54]. The spectra on this system and its analogues ought to be described through one set of geometrical factors (common for SA and TSA) and four D parameters: D^8_{SA}, D^9_{SA}, D^9_{TSA}, for SA and TSA, without or with inner sphere water (CN = 8 or 9). Thus one should actually observe four sets of signals, corresponding to the four situations (using the nomenclature of e.g. Ref. [54], these are M', m', M, m). The equilibrium between the capped and non-capped forms is comparatively fast: its exchange rate can be very roughly estimated between 10^6 and 10^7 s^{-1} [49], which justifies that provided D^8_{SA} and D^9_{SA} are not too different, the square antiprismatic form should actually give rise to one set of exchange broadened resonances; so would the TSA. This is exactly what is observed. Closely similar are the ligands based on hydroxyethyl and hydroxypropyl side chains and their Ln^{3+} complexes, THED [55], and THP [53], active in nucleic acid cleavage [56]. A remarkable aspect of these two complexes is the enhanced acidity of the hydroxyls, induced by the Ln^{3+} binding: $pK_a = 7.7$ has been reported for the first deprotonation of Eu(THP) [57].

Table 6
Experimental linewidths (Hz) for the two isomers of Yb DOTMA$^-$

Proton	$\Delta\nu$ (SA)	$\Delta\nu$ (TSA)
A_1	170	112
E_2	75	42
E_1	76	45
M	56	25
A_1	103	72
C	107	85

In the case of [Yb(DOTAMPh)]$^{3+}$, analogue to the system of Fig. 7, we observed a continuous change in spectral width upon adding DMSO to a CD_3CN solution, in agreement with the sensitivity of D to the axial ligand. Simultaneously, the lines underwent a remarkable broadening process, which reverted once an excess of DMSO had been added. Remarkably, on lowering the temperature, we were able to catch the two spectra that can be attributed to the DMSO- and CD_3CN-ligated forms [58]. It is worth recalling that, to the best of our knowledge, the complex [Yb(DOTAMPh)]$^{3+}$ does not give rise to a SA–TSA equilibrium.

Some lanthanide complexes endowed with a C_4 axis or analogous to those presented above have been used for molecular recognition. Recall the work of Aime, Parker and coworkers, who took advantage of systems closely similar to [Yb(DOTAMPh)]$^{3+}$, as depicted in Fig. 18 [59].

It is apparent that the coordination vacancy of the macrocyclic chelate, leaves Yb^{3+} open to the reversible binding of biologically relevant oxyanions, yielding systems able to spectroscopically report the environment composition. In close analogy to the discussion above in Sections 2.3.1 and 3.1, the strong sensitivity of the NIR (and NMR, as well) spectrum may lead to functional systems, to be used as spectroscopic probes or even as fluorescent stains in microscopy.

Complexes structurally similar to those described above found applications in emission spectroscopy, by realising so-called antenna systems, i.e. complexes where the ligand contains a suitable chromophore, absorbing in the UV and transferring energy to the lanthanide, which finally emits [22]. This arrangement overcomes the intrinsic weakness of lanthanide extinction coefficients because the light is captured by an efficient organic chromophore, and at the same time can exploit the wide emission spectrum obtained by changing the Ln^{3+} ion: from blue (Ce and Tm) to near IR (Nd, Er, Yb) (Fig. 19).

Lanthanide fluorescence is usually strongly sensitive to the presence of inner sphere water molecules, which efficiently quench it. This makes it possible to modulate the spectro-

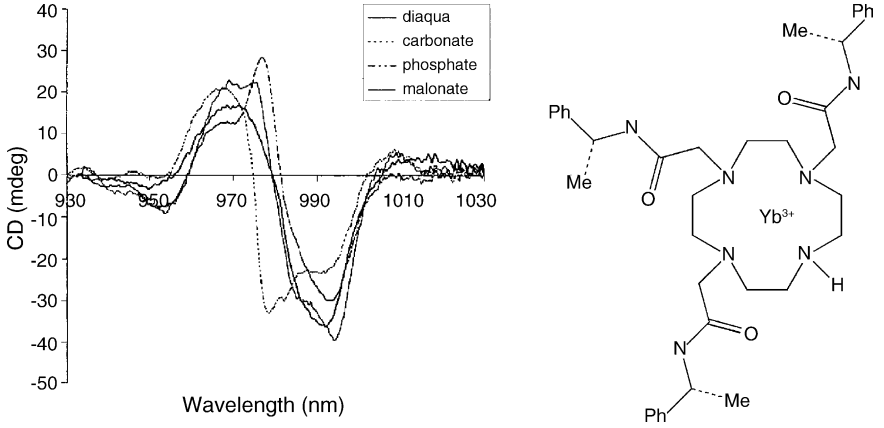

Fig. 18. NIR–CD spectra of ternary adducts, involving the Yb^{3+} complex depicted on the right, and diaquo, carbonate, phosphate or malonate [59].

scopic response of the complexes, which can be off, in the presence of H_2O or on, when it is excluded. An application to nucleic acids can be found in Ref. [23]. Very recently, Quici et al. described the sensitised Eu^{3+} and Er^{3+} visible and NIR emission, using phenanthroline as the capturing chromophore in a DOTA-analogue complex [60].

This work with lanthanide systems has already lent itself to applications, as sensors for biologically relevant substrates [61]. Tsukube and co-workers demonstrated that Ln^{3+} porphyrins, soluble in organic solvents, can extract α-amino acids from water [62]. The mechanism proposed for this interaction is once more an axial coordination, whereupon a ternary adduct is formed. The porphyrin itself is achiral and therefore it has a vanishing CD spectrum both around the Ln^{3+}-centred transitions and around the Soret band, which is the most prominent spectral feature of the organic moiety and falls at 420–440 nm. On the contrary, once the enantiopure amino acid has been extracted, one observes the appearance of Cotton effects in the Soret region, which proves the formation of a stereodefined adduct. Interestingly, all L-α-amino acids give rise to a bisignate CD doublet with negative band at lower energy and a positive one at shorter wavelengths. The existence of both the amino and carboxyl groups close to one another, is essential, as demonstrated through the use of dipeptides: in this case much weaker CD spectra are measured, in agreement with the longer distance between the two functional groups. In all cases, there is a 1:1 ratio between the amino acid moiety and the porphyrin, as shown by titration curves.[8]

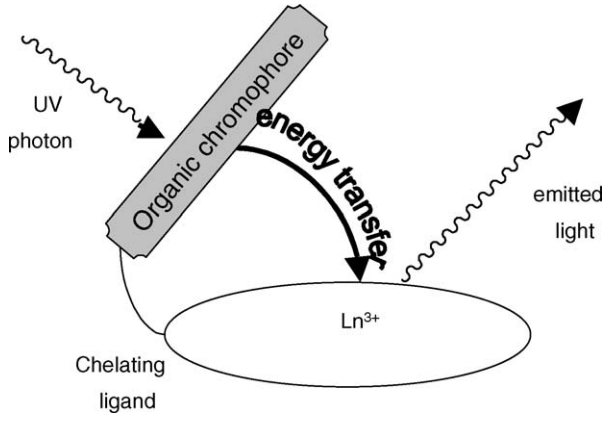

Fig. 19. Schematic representation of an antenna-complex.

When the parent complex is made chiral through the use of an enantiopure diketonate as the axial ligand, it exhibits a certain degree of recognition towards the various stereoisomers of the dipeptide alanylalanine (Ala–Ala).

A point, which surely deserves further investigation, is the origin of the spectral features of the Soret band of the ternary adduct. In the absorption spectrum two components are clearly recognised with an apparent splitting of about 10 nm (≈550 cm^{-1}). The amplitudes of these bands are remarkably different, with a ratio of about 0.25. In exact correspondence with these, there are the extreme points of the CD spectrum, which features two Cotton effects of opposite *and equal* rotational strengths (Fig. 20).

The whole situation is closely similar to an exciton coupled system, where two like chromophores interact through space. If this similarity holds, the adduct must contain at least two porphyrins, which is with the observation of a 1:1 ratio recalled above. We hope that further studies will shed more light on the structure of this promising system.

The existence of large aggregates involving many lanthanide chelates is neither new nor unexpected [63] and even macrocyclic ligands, where the lanthanide is clearly buried at the centre of an organic cage can give rise to supramolecular systems. This has been reported again by Tsukube for the cholesteryl derivative of DOTA shown in Ref. [64].

3.4. Dynamic symmetry

Many studies of monodentate ligands bound to shift reagents are reported in the literature and a complete survey definitely goes beyond our scope. Historically, shift reagents

[8] Each molecule of cystine, which contains two α-amino acid portions, binds two porphyrins.

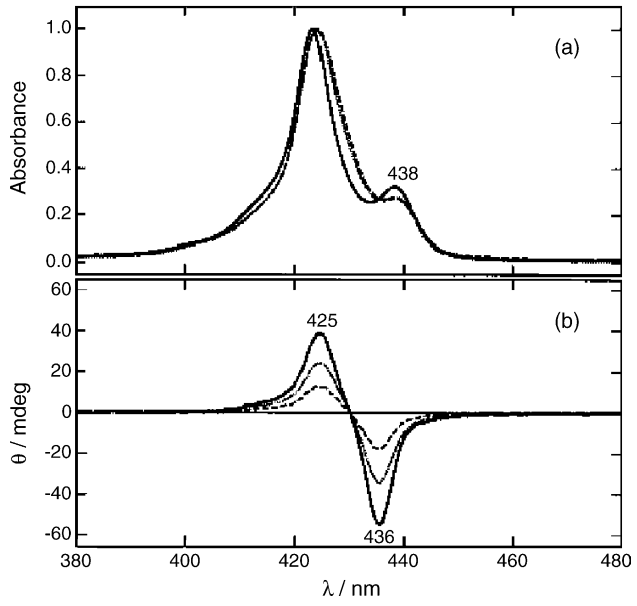

Fig. 20. Absorption (a) and CD (b) spectra of the ternary complex of Gd^{3+} tetraphenylporpyrin, L-phenylglycine and a diketonate, X; X = acetylacetonate (—); methyl acetylacetonate (· · ·); dipivaloyl methanate (- - -) [62].

like $Ln(dpm)_3^{3-}$, or its fluorinated analogue $Ln(fod)_3^{3-}$ were used together with simple rigid systems, like pyridine, picoline, borneol [17]. These studies aimed at demonstrating the power and limitations of the use of lanthanide reagents for structure determination and stereochemical analysis in solution. Thus, the first objective was evaluating the contact contribution and validating McConnel–Robertson equation (20). Naturally the whole complex is not axial, but it is dynamically symmetrised by the fast rotation along the C_3 of the shift reagent.

The use of shift reagents to investigate organic stereochemistry is still lively, as witnessed by the series of papers from Abraham and Sancassan [65]. In one of the latest reports, for example, these authors dealt with a classical conformational question: five-membered rings. Looking at cyclopentanol complexes with $Yb(fod)_3^{3-}$, they tried different conformers of the five-membered rings, and found that the best agreement between experimental and calculated (through McConnell–Robertson relation) δ^{pc} is achieved when the predominant role is assigned to an envelope conformation with the hydroxyl in axial position at the flap of the envelope. The second part of the paper concerns 1,2-cyclopentadiol, which was considered to bind the lanthanide only through one oxygen atom at a time. The results may take a different perspective on account of the wide literature concerning association between 1,2-diols and lanthanide diketonates, where chelation of the lanthanide is demonstrated [66]. This latter subject will be reviewed below in this section. In spite of the interest and potential of the method, we want to stress a general *caveat*: for non-rigid systems, there are at least two orders of problems when investigating the conformation (or its distribution) through shift reagents; in the first place, the reagent may bind preferentially to one of the conformers, letting it play a dominant role in the observed LIS and LIR; secondly, the minimum energy geometry (or a manifold of) may be seriously altered by the presence of such a bulky group as the lanthanide complex.

A recent report deals with the complex between chiral cobalamin derivatives and $Ln(DPA)_3^{3-}$ [16]. In this work, mentioned above in Section 2.1.2, the authors found that the X-ray structure of the axial ligands provides a set of coordinates, which is completely satisfactory to account for the geometry of the complex. This means that the structure of the derivatives is not altered following interaction with the lanthanide. Moreover, they apply Eq. (28) to determine the mole fraction of the bound cobalamin derivative, by estimating the anisotropy factor D from that of *free* $Tb(DPA)_3^{3-}$. This assumption seems justified in view of the electrostatic nature of the bond, where the positive cobalamin binds to the anionic $Tb(DPA)_3^{3-}$ with a (weak) outer sphere coordination. As discussed above, lanthanide diketonates rapidly switch between two enantiomeric conformations Λ and Δ. These two become diastereomeric in the presence of the chiral elements of vitamin B_{12} derivatives. Consequently, an asymmetric transformation takes place, leading to the prevalence of one enantiomer of the lanthanide diketonate. This is conveniently characterised through CD spectroscopy of the Nd^{3+} analogue, as demonstrated in Fig. 21.

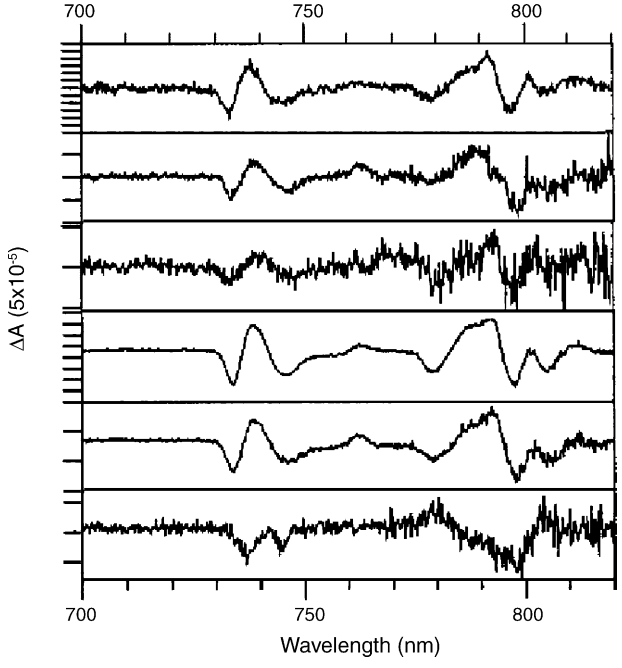

Fig. 21. Induced circular dichroism spectra of 10 mM $Nd(DPA)_3^{3-}$ in water upon the addition of (from top to bottom) H_2OCbl^+ (10 mM, pH 6.7), CNCbl (15 mM), $(CN)_2Cbi$ (26 mM), dimethyl-L-tartrate (DMT, 1.5 M, pH 7.5), Bovine serum albumin (BSA, 3 mM, pH 7.8) (H_2OCbl^+: aquacobalamin; CNCbl: cyanocobalamin; $(CN)_2Cbi$: dicyanocobalamide). Lowest plot: induced circular dichroism for $Nd(TTHA)_3^{3-}$ (20 mM) upon addition of bovine serum albumin (3 mM, pH 7.5) (TTHA: triethylene tetramine hexacetic acid) [16].

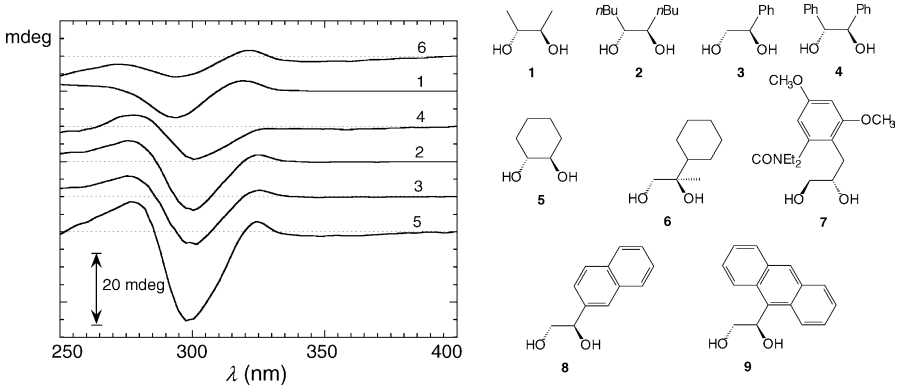

Fig. 22. UV–CD spectra recorded on 1:1 mixtures of $Yb(fod)_3^{3-}$ and chiral diols whose structures are depicted on the right [67].

By comparing the Nd^{3+} Vis–CD spectra of their derivatives with those of structurally known systems, the authors demonstrate that the three corrinoids induce the same chirality in $Nd(DPA)_3^{3-}$, whose prevailing enantiomer is Δ, and the relative amounts of enantioselectivity of hydro, cyanocobalamin and dicyanocobalamide. One more point highlighted by this work is the enantioselective binding of $Ln(DPA)_3^{3-}$ to serum albumin. Another application where the interplay of NMR and CD leads to a better understanding of functional systems is offered by the complex formed in situ when chiral diols bind axially to $Yb(fod)_3^{3-}$ [67]. It has been known since 1975 that Ln^{3+} diketonates offer a tool for determining the absolute configuration of diols and aminoalcohols [66]. Simply upon mixing the two systems, one obtains a complex where the chirality of the axial ligand induces stereodifferentiation of the two enantiomeric conformations of the $(fod)_3$ units. In many relevant cases the diols (or aminoalcohols) are devoid of strong absorptions in the Vis–UV, thus they are not amenable to a direct chiroptical investigation. On the contrary, the diketonate moiety has a strong absorption band centred around 300 nm and polarised along the O–O direction. In the propeller shaped $Yb(fod)_3^{3-}$ this would lead to a CD spectrum dominated by the exciton coupling of these transitions and appearing as a dissignate couplet (a sequence of two bands of opposite sign with the crossover point in close proximity to the absorption maximum). The situation is more complex, as demonstrated by the appearance of the UV–CD spectra for a series of structurally similar diols, shown in Fig. 22, where the couplet feature is not easily recognised. On the other hand, NIR–CD of Yb^{3+} clearly reveals a strong substrate-dependence.

In spite of this precaution, a reliable empirical correlation between the sign of the CD at 300 and 978 nm and the chirality of the diol can be drawn (negative at both wavelengths ↔ (*R*)- or (*R*,*R*)-configuration). Again with the aid of McConnell–Robertson equation (20), the analysis of the pseudocontact shifts measured on the 1,2-diol protons demonstrate unambiguously a well defined mode of chelation, where Yb participates in a five-membered ring, together with the two hydroxyl oxygen atoms and the two carbinol carbon atoms. The most bulky substituents on the diol tend to occupy a pseudoequatorial position. This result is not unexpected, it is nonetheless based solely on the analysis of experimental data. The evidence of relevant exchange processes (partly also involving water) is striking by looking at the linewidths of the ^1H NMR signals, which easily exceed 100 Hz, to be compared with the expected value of 8.3 Hz of Table 1. In fact, in order to obtain a dynamic axial symmetry, justifying the use of McConnel–Robertson equation, one must invoke a fast reorientation between the C_3-

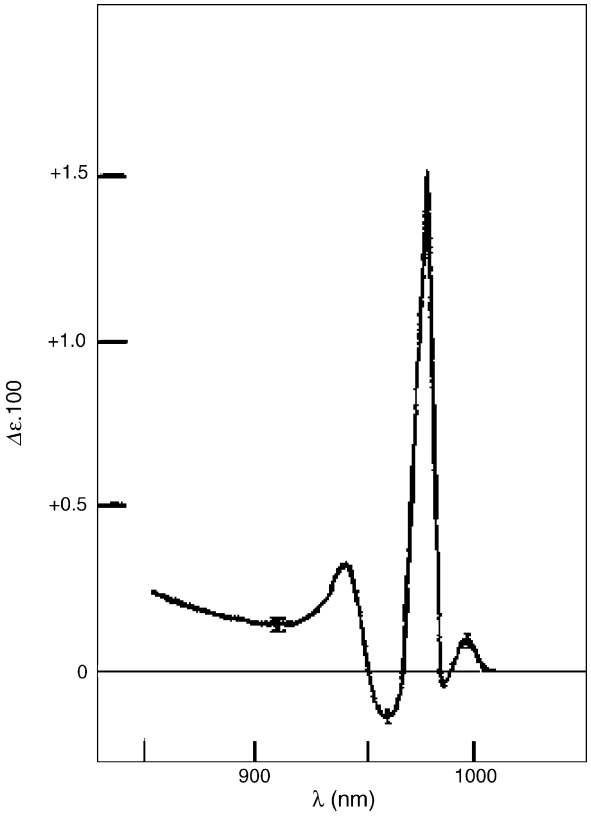

Fig. 23. NIR–CD spectrum of a rifampicin and Yb^{3+} in MeOH/water [69].

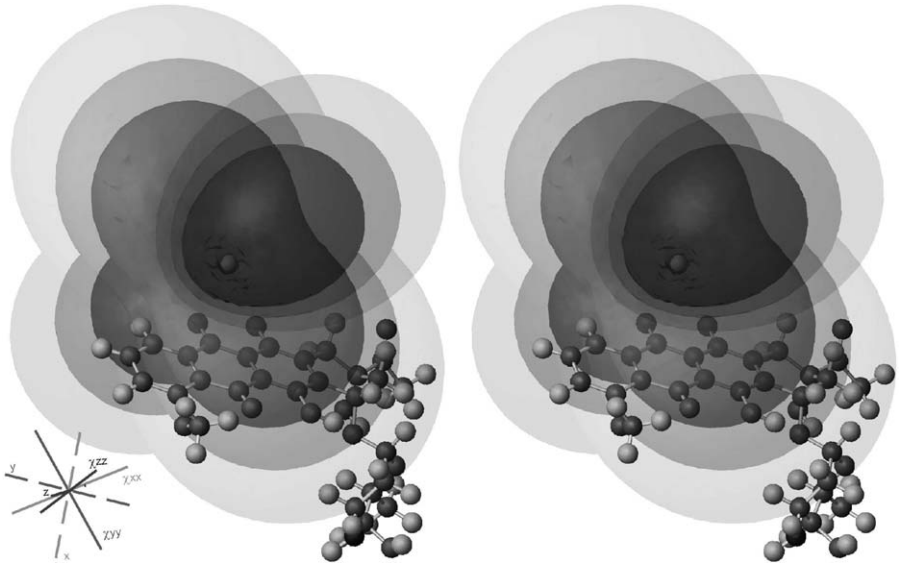

Fig. 24. Stereo view representation of the adduct between adriamycin and Yb^{3+} and representation of the pseudocontact shift effect: the surfaces depicted represent regions where the nuclei experience positive (darker shades) and negative shifts [58].

symmetric unit and the additional ligand, which is bidentate in the present case.

3.5. Non-symmetric complexes

Finally we wish to briefly comment on some cases where a "naked" lanthanide ion is used as spectroscopic probe to investigate the stereochemistry of biologically relevant molecules. This line of research has deep roots in the observation that Ln^{3+} have coordination properties, similar to those of Ca^{2+} and Mg^{2+}. These alkali earth ions are responsible for many important processes in living systems but are hardly amenable to spectroscopy, owing to their silentness [68]. The combination of NMR and optical, especially CD, spectroscopy provides detailed information on the structure of the cation binding site of biomolecules. NIR–CD of Yb^{3+}, for example provides immediate evidence of the formation of a stereodefined complex with rifamycin antibiotics, as shown in Fig. 23 [69].

More recently, the developments in paramagnetic NMR discussed in Part I, supplied a more complete background for such analysis. The investigations of Lenkinski [70] and Ming [5] on the anthracycline/Yb^{3+} interactions allowed us a more detailed study, whereby the full magnetic anisotropy tensor of Yb^{3+} bound to the antibiotic adriamycin was determined, as shown in Fig. 24 [6].

The field of protein–lanthanide interactions is currently exploding: the number and quality of reports in the field improved every month. The combination of large hyperfine shifts, comparatively narrow linewidths, joined to a versatile choice of the most suited Ln^{3+} to the problem account for this popularity. Even a simplified discussion of this subject would take us too far from the scope of the present work.

4. Conclusions

We have discussed selected methods and examples of the study of chiral lanthanide complexes. These systems find applications in several fields of chemistry and biochemistry, largely owing to the plasticity of Ln^{3+} ions. Flexible coordination number, electrostatic nature of chemical bond, strong Lewis acidity are a few determinant properties. On top of this, rich and varied spectroscopic responses rooted in the unusual properties of f-electrons, make these ions extraordinary structural and functional probes. We believe that much more will be unearthed and we hope that this small contribution will encourage chemists to visit this fascinating field.

Acknowledgements

Financial support from MIUR (PRIN Stereoselezione in Sintesi Organica) is gratefully acknowledged. The authors are indebted to Drs. G. Pintacuda, M. Lelli and G. Pescitelli for helpful discussions.

References

[1] I. Bertini, C. Luchinat, NMR of paramagnetic substances, Coord. Chem. Rev. 150 (Special issue) (1996).
[2] (a) J.A. Peters, J. Huskens, D.J. Raber, Prog. NMR Spectrosc. 28 (1996) 283–350;
(b) C. Piguet, C.F.G.C. Geraldes, in: K.A. Gsheidener Jr., J.-C.G. Bünzli, V.K. Pecharsky (Eds.), Handbook of Physics and Chemistry of Rare Earths, vol. 33, Elsevier Science, 2003, pp. 353–463.
[3] A.J. Freeeman, R.E. Watson, Phys. Rev. 127 (1962) 2058–2075.
[4] (a) S. Aime, M. Botta, G. Ermondi, Inorg. Chem. 31 (1992) 4291–4299;

(b) S. Hoeft, K. Roth, Chem. Ber. 126 (1993) 869–873;
(c) V. Jacques, J.F. Desreux, Inorg. Chem. 33 (1994) 4048–4053;
(d) L. Di Bari, G. Pintacuda, P. Salvadori, Eur. J. Inorg. Chem. (2000) 75–82.
[5] X. Wei, L.-J. Ming, Inorg. Chem. 37 (1998) 2255–2262.
[6] L. Di Bari, G. Pintacuda, S. Ripoli, P. Salvadori, Magn. Reson. Chem. 40 (2002) 396–405.
[7] L. Perrin, R.K. Gipe, J. Am. Chem. Soc. 106 (1984) 4036, for an application to lanthanide complexes, see for example Ref. [4c].
[8] B. Bleaney, J. Magn. Reson. 8 (1972) 91–100.
[9] V.S. Mironov, Y.G. Galyametdinov, A. Ceulemans, C. Gorller-Walrand, K. Binnemans, J. Chem. Phys. 116 (2002) 4673–4685.
[10] J.H. Forsberg, R.M. Delaney, Q. Zhao, G. Harakas, R. Chandran, Inorg. Chem. 34 (1995) 3705–3715.
[11] M.D. Kemple, B.D. Ray, K.B. Lipkowitz, F.G. Prendergast, B.D.N. Raot, J. Am. Chem. Soc. 110 (1988) 8275–8287.
[12] J. Lisowski, J.L. Sessler, V. Lynch, T.D. Mody, J. Am. Chem. Soc. 117 (1995) 2273–2285.
[13] J. Ren, A.D. Sherry, J. Magn. Reson. B 111 (1996) 178–182.
[14] J. Ren, S. Zhang, A.D. Sherry, C.F.G.C. Gerades, Inorg. Chim. Acta 339 (2002) 273–282.
[15] (a) J. Reuben, G.A. Elgavish, J. Magn. Reson. 39 (1980) 421–430;
(b) J. Reuben, J. Magn. Reson. 50 (1982) 233–236;
(c) C. Platas, F. Avecilla, A. de Blas, C.F.G.C. Geraldes, T. Rodríguez-Blas, H. Adams, J. Mahía, Inorg. Chem. 38 (1999) 3190–3199.
[16] S.C.J. Meskers, H.P.J.M. Dekkers, Spectrochim. Acta: A 55 (1999) 1837–1855.
[17] (a) O. Hofer, Top. Stereochem. 9 (1980) 111–197;
(b) J.D. Roberts, G.E. Hawkes, J. Husar, A.W. Roberts, D.W. Roberts, Tetrahedron 30 (1974) 1833–1884;
(c) F. Inagaki, T. Miyazawa, Prog. NMR Spectrosc. 14 (1980) 67–111.
[18] L. Banci, I. Bertini, K.L. Bren, M.A. Cremonini, H.B. Gray, C. Luchinat, P. Turano, J. Biol. Inorg. Chem. 1 (1996) 117–126.
[19] (a) J.F. Desreux, Inorg. Chem. 19 (1980) 1319–1324;
(b) H.G. Brittain, J.F. Desreux, Inorg. Chem. 23 (1984) 4459–4466;
(c) S. Aime, M. Botta, G. Ermondi, Inorg. Chem. 31 (1992) 4291–4299.
[20] F.S. Richardson, Inorg. Chem. 19 (1980) 2806–2812.
[21] L. Di Bari, G. Pintacuda, P. Salvadori, J. Am. Chem. Soc. 122 (2000) 5557–5562.
[22] H. Maas, A. Currao, G. Calzaferri, Angew. Chem. Int. Ed. Eng. 41 (2002) 2495–2497.
[23] A. Beeby, R.S. Dickins, S. Faulkner, D. Parker, J.A.G. Williams, Chem. Commun. (1997) 1401–1402.
[24] (a) A.P. deSilva, H.Q.N. Gunaratne, T.E. Rice, Angew. Chem. Int. Ed. Eng. 35 (1996) 2116–2118;
(b) D. Parker, K. Senanayake, J.A.G. Williams, Chem. Commun. (1997) 1777–1778;
(c) T. Gunnlaugsson, D. Parker, Chem. Commun. (1997) 511–512;
(d) A. Lobnik, N. Majcen, K. Niederreiter, G. Uray, Sens. Actuators B 74 (2001) 200–206;
(e) M. Woods, A.D. Sherry, Inorg. Chem. 42 (2003) 4401–4408;
(f) T. Gunnlaugsson, J.P. Leonard, K. Senechal, A.J. Harte, J. Am. Chem. Soc. 125 (2003) 12062–12063.
[25] D. Parker, P.K. Senanayake, J.A.G. Williams, J. Chem. Soc., Perkin Trans. 2 (1998) 2129–2139.
[26] (a) P. Atkinson, Y. Bretonniere, D. Parker, Chem. Commun. (2004) 438–439;
(b) A.L. Jenkins, O.M. Uy, G.M. Murray, Anal. Commun. 34 (1997) 221–224;
(c) R.S. Dickins, T. Gunnlaugsson, D. Parker, R.D. Peacock, Chem. Commun. (1998) 1643–1644;
(d) T. Yamada, S. Shinoda, H. Tsukube, Chem. Commun. (2002) 1218–1219.
[27] T. Gunnlaugsson, J.P. Leonard, Chem. Commun. (2003) 2424–2425.
[28] (a) V.W.W. Yam, K.K.W. Lo, Coord. Chem. Rev. 184 (1999) 157–240;
(b) L.J. Govenlock, C.E. Mathieu, C.L. Maupin, D. Parker, J.P. Riehl, G. Siligardi, J.A.G. Williams, Chem. Commun. (1999) 1699–1700;
(c) G. Bobba, S.D. Kean, D. Parker, A. Beeby, G. Baker, J. Chem. Soc., Perkin Trans. 2 (2001) 1738–1741;
(d) G. Bobba, J.C. Frias, D. Parker, Chem. Commun. (2002) 890–891.
[29] (a) P.S. May, D.H. Metcalf, F.S. Richardson, R.C. Carter, C.E. Miller, R.A.J. Palmer, Luminescence 51 (1992) 249–268;
(b) K.A. Schoene, J.R. Quagliano, F.S. Richardson, Inorg. Chem. 30 (1991) 3803–3812.
[30] E. Castiglioni, Book of Abstracts of the Sixth International Conference on Circular Dichroism, Pisa, 1997. See also the URL: http://digilander.libero.it/ecssrl.
[31] F.S. Richardson, Inorg. Chem. 19 (1980) 2806–2812.
[32] T.A. Babushkina, V.F. Zolin, L.-G. Koreneva, J. Magn. Reson. 52 (1983) 169–181.
[33] W.DeW. Horrocks, J.P. Sipe, Survey 93 (1971) 6800–6804.
[34] I. Bertini, M.B.L. Janik, Y.-M. Lee, C. Luchinat, A. Rosato, J. Am. Chem. Soc. 123 (2001) 4181–4188.
[35] R.S. Dickins, D. Parker, J.I. Bruce, D.J. Tozer, J. Chem. Soc., Dalton Trans. (2003) 1264–1271.
[36] L. Di Bari, G. Pintacuda, P. Salvadori, R.S. Dickins, D. Parker, J. Am. Chem. Soc. 122 (2000) 9257–9264.
[37] C. Rosini, L. Franzini, A. Raffaelli, P. Salvadori, Synthesis (1992) 502–517.
[38] J. Lisowski, S. Ripoli, L. Di Bari, Inorg. Chem. 43 (2004) 1388–1394.
[39] (a) J. Lisowski, Magn. Reson. Chem. 37 (1999) 287–294;
(b) J. Lisowski, P. Starynowicz, Polyhedron 19 (2000) 465–469.
[40] M. Shibasaki, N. Yoshikawa, Chem. Rev. 102 (2002) 2187–2209.
[41] H.C. Aspinall, Chem. Rev. 102 (2002) 1807–1850.
[42] L. Di Bari, M. Lelli, G. Pintacuda, G. Pescitelli, P. Salvadori, J. Am. Chem. Soc. 125 (2003) 5549–5558.
[43] H.C. Aspinall, Organometallics 19 (2000) 5416–5423.
[44] L. Di Bari, G. Pescitelli, P. Salvadori, J. Am. Chem. Soc. 121 (1999) 7998–8004.
[45] L. Di Bari, M. Lelli, P. Salvadori, Chem. Eur. J. 10 (2004) 4594–4598.
[46] J.J. Lessmann, W.DeW. Horrocks, Inorg. Chem. 39 (2000) 3114–3124.
[47] M. Cantuel, G. Berardinelli, G. Muller, J.P. Riehl, C. Piguet, Inorg. Chem. 43 (2004) 1840–1849.
[48] (a) J.F. Desreux, Inorg. Chem. 19 (1980) 1319–1324;
(b) H.G. Brittain, J.F. Desreux, Inorg. Chem. 23 (1984) 4459–4466;
(c) S. Aime, M. Botta, G. Ermondi, Inorg. Chem. 31 (1992) 4291–4299.
[49] D.H. Powell, O.M. Ni Dhubhghaill, D. Pubanz, L. Helm, Y.S. Lebedev, W. Schlaepfer, A.E. Merbach, J. Am. Chem. Soc. 118 (1996) 9333–9346.
[50] E.L. Eliel, S.H. Wilen, L.N. Mander, Stereochemistry of Organic Compounds, Wiley, New York, USA, 1994, p. 769.
[51] L. Di Bari, G. Pintacuda, P. Salvadori, Eur. J. Inorg. Chem. (2000) 75–82.
[52] R.S. Ranganathan, N. Raju, H. Fan, X. Zhang, M.F. Tweedle, J.F. Desreux, V. Jacques, Inorg. Chem. 41 (2002) 6856–6866.
[53] K.O.A. Chin, J.R. Morrow, C.H. Lake, M. Rowen Churchill, Inorg. Chem. 33 (1994) 656–664.
[54] S. Aime, M. Botta, M. Fasano, M.P.M. Marques, C.F.G.C. Geraldes, D. Pubanz, A.E. Merbach, Inorg. Chem. 36 (1997) 2059–2068.
[55] J.R. Morrow, K.O.A. Chin, Inorg. Chem. 32 (1993) 3357–3361.
[56] D.M. Corsi, L. Vander Elst, R.N. Muller, H. van Bekkum, J.A. Peters, Chem. Eur. J. 7 (2001) 1383–1389.
[57] B.F. Baker, H. Khalili, N. Wei, J.R. Morrow, J. Am. Chem. Soc. 119 (1997) 8749–8755.
[58] G. Pintacuda, Ph.D. Thesis, Scuola Normale Superiore, Pisa, 2004.

[59] R.S. Dickins, S. Aime, A.S. Batsanov, A. Beeby, M. Botta, J.I. Bruce, J.A.K. Howard, C.S. Love, D. Parker, R.D. Peacock, H. Puschmann, J. Am. Chem. Soc. 124 (2002) 12697–12705.
[60] S. Quici, G. Marzanni, A. Forni, G. Accorsi, F. Barigelletti, Inorg. Chem. 43 (2004) 1294–1301.
[61] (a) H. Tsukube, S. Shinoda, Chem. Rev. 102 (2002) 2369–2403;
(b) H. Tsukube, S. Shinoda, H. Tamiaki, Coord. Chem. Rev. 226 (2002) 227–234.
[62] H. Tamiaki, S. Unno, E. Takeuchi, N. Tameshige, S. Shinoda, H. Tsukube, Tetrahedron 59 (2003) 10477–10483.
[63] Z. Zheng, Chem. Commun. (2001) 2521–2529.
[64] S. Shinoda, T. Okazaki, T. Nishimura, K. Hori, H. Tsukube, Chem. Commun. (2001) 976–977.
[65] (a) R.J. Abraham, R. Koniotou, F. Sancassan, J. Chem. Soc., Perkin Trans. 2 (2002) 2025–2030;
(b) R.J. Abraham, F. Sancassan, Encyclopedia of NMR, vol. 9, 2002, Chapter 5, p. 578, and references therein.
[66] J. Dillon, K. Nakanishi, J. Am. Chem. Soc. 97 (1975) 5417–5422.
[67] L. Di Bari, M. Lelli, G. Pintacuda, P. Salvadori, Chirality 14 (2002) 265–273.
[68] C.H. Evans, Biochemistry of the Lanthanides, Plenum Press, New York, 1990.
[69] P. Salvadori, C. Bertucci, C. Rosini, J. Am. Chem. Soc. 106 (1984) 2439–2440.
[70] I.J. McLennan, R.E. Lenkinski, J. Am. Chem. Soc. 106 (1984) 6905–6909.